Sensitivity of Tropical Pacific Convection to Dry Layers at Mid- to Upper Levels: Simulation and Parameterization Tests

JAMES A. RIDOUT

Naval Research Laboratory, Monterey, California

(Manuscript received 24 October 2001, in final form 12 June 2002)

ABSTRACT

Numerical forecast experiments are carried out to investigate the implications of observed moisture variability in the tropical Pacific for deep convection. The study uses a series of quasi-cloud-resolving model forecasts with a triple-nested version of the Naval Research Laboratory's Coupled Ocean–Atmosphere Mesoscale Prediction System (COAMPS). The forecasts are carried out for a dry tongue episode in the tropical western Pacific in November 1998. During a 24-h forecast, a number of convective cells develop in an area of deep convection near the edge of the simulated dry tongue in the COAMPS 3-km mesh inner grid, which is located in the southern portion of the domain of the Tropical Ocean Global Atmosphere Coupled Ocean–Atmosphere Response Experiment (TOGA COARE) field program. The forecast is repeated multiple times using a moisture profile from a TOGA COARE dry tongue episode to modify the lateral boundary conditions for the 3-km mesh grid over layers of varying depth and altitude. The entrainment of drier air results in a 37% reduction in rainfall when the dry layer extends from the 600-hPa level to the model top. Tests show that entrainment of dry air at mid levels has a major impact in suppressing precipitation production due to cold rain processes. It should be noted that conditions where warm rain processes dominate are not addressed by the present experiments. Associated with the suppression of deep convection by dry layers in these forecasts, there is a large increase in stored buoyant energy. The presence of dry midtropospheric air may thus serve to help permit the buildup of buoyant energy for subsequent episodes of deep convection, such as associated with the onset of the Madden–Julian oscillation.

In order to investigate the ability of convective parameterizations to represent the moisture sensitivity observed in the COAMPS experiments, data from the COAMPS 3-km mesh grid were used for tests of convective parameterizations in both semiprognostic model (SPM) and single-column model (SCM) mode. Both the Emanuel and the Kain–Fritsch convective parameterizations are unable to account in the SPM tests for the reduction in rainfall and cloud-base mass flux obtained on the COAMPS 3-km mesh grid when dry lateral boundary conditions are imposed above the 600-hPa level. The results are consistent with the interpretation that inadequacies in the convective closure assumptions play a signficant role. Comparisons of updraft mass flux profiles in the SPM tests point to considerable sensitivity to the details of the implementation of the stochastic buoyancy-sorting model in these schemes. In the SCM tests, the parameterized rainfall amounts are better than in semiprognostic mode, but apparently too low in one case by a substantial amount. In addition, large errors are observed in the simulated stored buoyant energy. The convective schemes are shown to perform best for greater horizontal resolutions of the forcing data.

1. Introduction

The impact of entrainment of dry environmental air on atmospheric convection has been a topic of speculation and research for many years (Simpson 1983). The theory that entrainment of dry air can act to reduce parcel buoyancy and limit cloud vertical development was first formally proposed by Stommel (1947). Consistent with this reasoning is the suggested mechanism of ''preconditioning'' of the atmosphere for deep convection through moistening by shallow convection (e.g., Esbensen 1978; Johnson 1978). Because of the sensitivity of convection to the detailed structure and evolution of the earth's troposphere, the extent and significance of dry air entrainment is expected to vary considerably. Tests with an implementation of the stochastic buoyancy-sorting model of updraft/environment mixing of Raymond and Blyth (1986), for example, suggest that the impact of tropospheric dryness above the boundary layer depends to a substantial degree on parcel buoyancy (Kain and Fritsch 1990). Observations have been reported supporting a relationship between the occurrence of dry midlevel air and convective activity in both northern Florida (Fuelberg and Biggar 1994) and the tropical Pacific (Brown and Zhang 1997).

Numerical model experiments offer one avenue by which an improved understanding in this area can be obtained, and recent modeling studies have addressed

Corresponding author address: Dr. James A. Ridout, NRL-Monterey, 7 Grace Hopper Avenue, Stop 2, Monterey, CA 93943-5502.
E-mail: ridout@nrlmry.navy.mil

various facets of this issue. Gilmore and Wicker (1998), for example, describe the sensitivity of supercell morphology and evolution to midtropospheric moisture. Bryan and Fritsch (2000) describe a sensitivity of the organizational structure of midlatitude squall-line convection to the moisture of air above the 850-hPa level. Lucas et al. (2000) present results that suggest that tropical oceanic convection is most sensitive to environmental moisture below 700 hPa, where dryness can inhibit deep convection. Tompkins (2001) also presents evidence supporting the importance for tropical oceanic convection of moisture in the lower troposphere.

The implication of the cited modeling studies for the importance of moisture at low levels for tropical oceanic convection seems reasonable, especially within or near the source layer of air feeding into convective updrafts. At mid to upper levels, the focus of the present modeling effort, the effect of dry layers is expected to depend on parcel buoyancies within the updraft, as well as perhaps other factors such as wind shear, which may affect the rate of updraft/environment mixing. As indicated in the preceding discussion, possible evidence for the importance for tropical convection of dry layers at mid to upper levels is provided by the observational study of Brown and Zhang (1997). The study in question is based on data from the Tropical Ocean Global Atmosphere Coupled Ocean–Atmosphere Response Experiment (TOGA COARE; Webster and Lucas 1992). Brown and Zhang (1997) present differing analyses of the relationships between cloud-top height and atmospheric moisture, and between precipitation and moisture. The connection between cloud-top height and moisture is addressed using satellite and sounding data for three island sites within the region of the Intensive Flux Array (IFA). The data show what appears to be a good correlation between cloud-top height and the vertically averaged relative humidity between 950 and 550 hPa. This observation supports the hypothesis that cloud development over the Tropics can be significantly limited by an extremely dry atmosphere. These data, however, are not inconsistent with the possibility that the most significant moisture variations are those in the lower portion of the layer examined.

The precipitation/moisture statistics presented by Brown and Zhang (1997) are perhaps more conducive to efforts at establishing a role for midlevel moisture than are the cloud-top height data. The moisture data are compiled for four different layers. For the two layers that lie below 850 hPa, the correlation between rainfall and relative humidity was not very great in the TOGA COARE IFA region. On the other hand, a correlation of 0.65 was reported for data filtered with a 5-day running mean between rainfall and average humidity in the layer between 850 and 200 hPa. The plotted data (Brown and Zhang 1997) suggest the best correlation between rainfall and relative humidity is for the upper portion of this range (550 to 200 hPa). Rainfall tends to be greater when the mid- to upper-level moisture is greater. Whether this relationship reflects an inhibition of precipitation associated with episodes of dry upper-level air or simply the enhancement of moisture at upper levels in the presence of increased convection is not clear from the data (Brown and Zhang 1997). A combination of these two processes may in fact be at work.

To the degree that moisture variability is a causative factor of variability in deep convection (rather than simply a result of such variability), it can be regarded as what is sometimes referred to as an atmospheric ''control'' or ''regulation'' mechanism. Although such ''causative'' factors may, in truth, be simply portions of a grander, more complex scheme, the concept of a process as a control or regulator can serve as a helpful working hypothesis, while research progresses toward a fuller understanding. Addressing the potential role of moisture variability in the Tropics as a regulator of convection, Brown and Zhang (1997) suggested that deep convection in the Tropics may act to induce observed influxes of dry air from the subtropics to the Tropics, which would in turn act to inhibit convection. Such influxes of dry air, so-called dry tongues, occur on scales of the order of hundreds of kilometers and persist for several days (e.g., Numaguti et al. 1995; Sheu and Liu 1995; Mapes and Zuidema 1996). Their coincidence with periods of suppressed convection has made them suspect as the cause for such ''drought'' periods (e.g., Yoneyama and Fujitani 1995; Mapes and Zuidema 1996; Lucas and Zipser 1996). In order to obtain insight into the potential for this type of control, in section 2 of the present study the impact on cloud growth of moisture variations of the nature of those associated with dry tongue episodes in the tropical Pacific is investigated by means of a series of quasi-cloud-resolving-scale numerical forecast experiments. These forecasts are carried out using a version of the Naval Research Laboratory's Coupled Ocean–Atmosphere Mesoscale Prediction System (COAMPS™; Hodur 1997).[1]

Because numerical modeling studies of the large-scale properties of the atmospheric general circulation currently rely on parameterized treatments of deep convection, it is desirable to understand the degree to which parameterizations represent sensitivities such as those investigated in the present work. Deficiencies in the schemes can thus be brought to light and hopefully addressed, or at least understood. The importance of this effort is highlighted by the fact that numerical models continue to exhibit problems representing key aspects of the tropical circulation such as the Madden–Julian oscillation (MJO; e.g., Slingo et al. 1996; Jones et al. 2000; Maloney and Hartmann 2001), for which parameterized convection may be responsible. Convective parameterization tests can also potentially provide information concerning the validity of the assumptions that form the basis for the schemes. The variety of convec-

[1] COAMPS is a trademark of the Naval Research Laboratory.

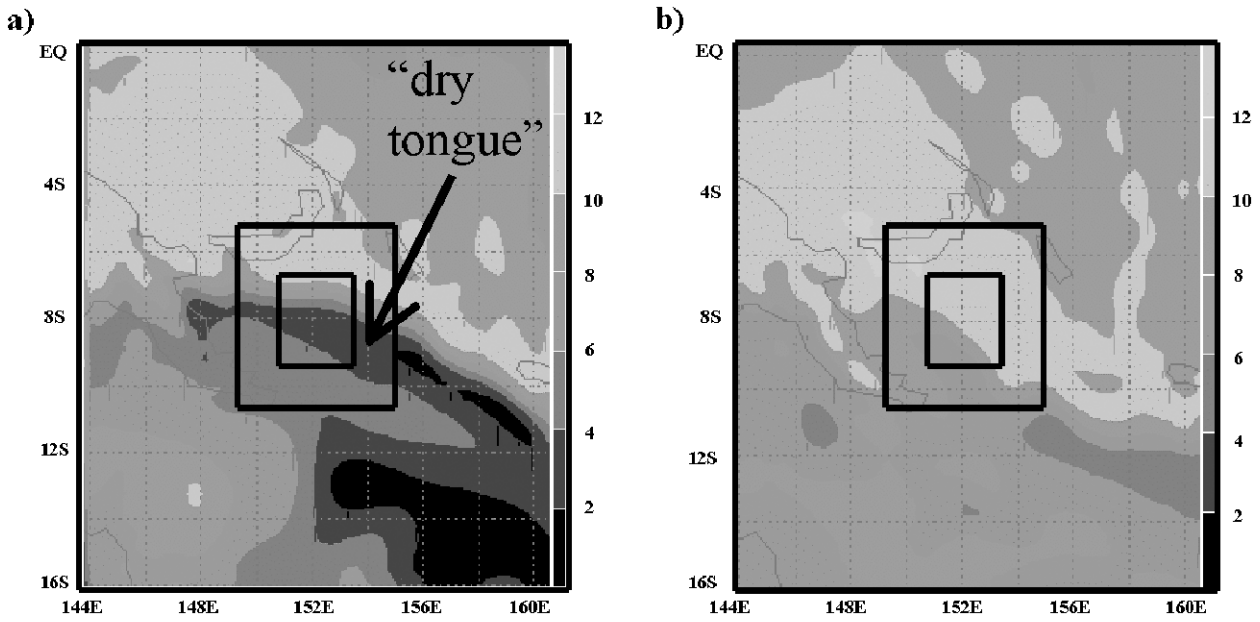

FIG. 1. Mixing ratio (g kg^{-1}) at 700 hPa for analyses at 0000 UTC on (a) 19 and (b) 21 Nov 1998. The location of the inner (3- and 9-km mesh) COAMPS grids are shown. The coarse (27 km) mesh grid domain is the entire region plotted.

tive closure formulations, for example, is evidence of the degree of uncertainty as to the convective response to atmospheric conditions over a range of scales (e.g., Arakawa and Schubert 1974; Kuo 1974; Fritsch and Chappell 1980; Emanuel and Zivkovic-Rothman 1999). Motivated by these considerations, the predictions of two convective schemes are assessed for the COAMPS forecasts presented in section 2. The schemes examined here are that of Emanuel (Emanuel 1991; Emanuel and Zivkovic-Rothman 1999) and that of Kain and Fritsch (1990). Both of these schemes include an implementation of the buoyancy-sorting mixing mechanism proposed by Raymond and Blyth (1986), so may be expected to have some success in representing the sensitivity of convection to moisture variability above cloud-base level.

The convective parameterization tests are carried out using a system described here for controlled experiments with model physics parameterizations in COAMPS. The method employed is to run the COAMPS nonhydrostatic forecast model at high resolution where convection is resolved, or nearly so, generating data that can be used off-line for tests in either a semiprognostic model (SPM) mode or a single-column model (SCM) mode. The reader is reminded that the difference between these two types of tests is simply that, in the SPM mode, the evolution of the atmospheric profile is prescribed, whereas in the SCM mode, the atmospheric profile evolves as determined by (prescribed) advective tendencies and the physics of the model (e.g., Randall et al. 1996). Petch and Dudhia (1998) have applied this basic technique, for example, in experiments with simulation data from the fifth-generation Pennsylvania State University–National Center for Atmospheric Research Mesoscale Model (PSU–NCAR MM5). This method has the obvious disadvantage of relying on what may be unrealistic model output for data. One advantage is that the horizontal resolution of the dataset used to run the physics tests can easily be modified, quite the contrary to observed data. Other advantages exist as well. For example, the environment used for the initial three-dimensional model forecasts can be modified, allowing for a look at the ability of parameterizations to account for a specific change in the environment. This feature is exploited in the present work for the moisture sensitivity experiments presented in section 2. The results of COAMPS SPM and SCM tests with both the Emanuel and Kain–Fritsch convective parameterizations are reported in section 3 using data from these experiments. Section 4 concludes with a discussion of the results and their implications.

2. COAMPS forecast experiments

The forecast experiments were carried out using a triple-nested version of COAMPS. The inner mesh in the forecasts has a horizontal dimension of 3 km, allowing for a somewhat crude resolution of deep convective circulations. During the 24-h focus period of these experiments, this fine-mesh grid is located in a region of deep convection near the edge of a dry tongue in a forecast by the outer (27 km) mesh grid in the western tropical Pacific in November 1998 (Fig. 1). It should be noted that the data needed to run the COAMPS forecasts for a TOGA COARE dry tongue case of interest are not available. The episode chosen

is similar to one that occurred in November 1992 during TOGA COARE in which dry air appears to move to the northeast from the subtropics into the equatorial region. The case modeled here was initially identified for this work using data from the National Centers for Environmental Prediction–National Center for Atmospheric Research (NCEP–NCAR) Climate Data Assimilation System (CDAS) Reanalysis Project (Kalnay and Jenne 1991; Kalnay et al. 1993). Several simulations were carried out for the November 1998 case. Because the COAMPS 3-km mesh grid, which was centered at 8°S and 152°E during the forecast experiments, was located near, but not within, the dry tongue, the moisture sounding was not representative of the dry tongue itself. The 3-km mesh was situated in an area of deep convection, and by carrying out experiments in which dry air above the boundary layer is allowed to advect into this mesh the impact on deep convection of enhanced evaporation could be investigated. The hypothesis to be tested relates to the discussion in section 1. If the simulated precipitation is only weakly sensitive to mid- to upper-level moisture perturbations, support would be obtained for the position that the observed correlation between moisture at those levels and precipitation during TOGA COARE is primarily due to the moistening of the environment associated with deep convection. On the other hand, considerable sensitivity in this regard would lend support to the view of moisture variability as a significant control mechanism for convective precipitation in the Tropics.

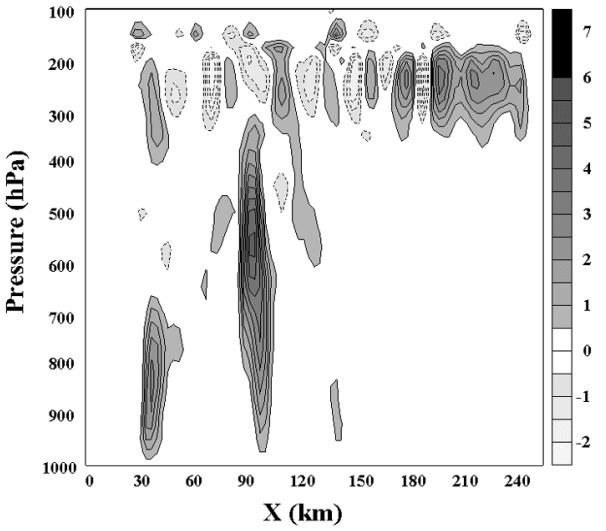

FIG. 2. East–west vertical cross section plot of vertical velocity (in m s^{-1}) through the COAMPS 3-km mesh grid (30 km north of the center of the grid) for Forecast CTL at approximately tau = 8 h.

a. COAMPS

The COAMPS forecast system consists of code for atmospheric data quality control, analysis, and initialization, as well as a nonhydrostatic atmospheric forecast model and a hydrostatic ocean model (Hodur 1997). Forecasts are carried out using lateral boundary conditions from the Navy Operational Global Atmospheric Prediction System (NOGAPS; Hogan and Rosmond 1991). For the present work, Davies (1976) boundary conditions are used, though other options are available. The inner nests are run without allowing for feedback to the parent nests. This treatment simplifies interpretation of the results, and test runs with the nest feedback turned on showed little effect on the moisture sensitivity investigated here. The physics package provides for some flexibility by means of user-selected options. For the present study, vertical subgrid-scale turbulent mixing is computed using the scheme of Mellor and Yamada (1974) and surface fluxes are computed using the treatment of Louis et al. (1982). Parameterized horizontal subgrid-scale turbulent mixing is neglected, supported by tests showing little impact on the present results. The convective parameterization of Kain and Fritsch (1990) is used for the 27-km mesh grid; otherwise convection is modeled explicitly. The standard microphysics scheme in COAMPS is that of Rutledge and Hobbs (1983), and includes a treatment of snow and cloud ice, as well as rain drops and cloud water. The research version of COAMPS used for this study employs, rather, a scheme developed by Ferrier (1988) so as to provide for a treatment of a graupel/hail phase as well. Radiation is treated following Harshvardhan et al. (1987), utilizing the diagnostic cloud parameterization of Slingo (1987).

b. Moisture sensitivity tests

For the present forecasts, the COAMPS model was spun up over a 3-day period using the data assimilation system and a cycle time of 12 h. The model was run with 30 vertical levels, and the 3-km mesh grid had 85 × 85 grid points in the horizontal. A 24-h forecast beginning at 0000 UTC on 21 November 1998 was initiated after the spinup period. In this forecast, denoted here as Forecast CTL, a number of deep convective cells develop in the 3-km mesh grid. The deepest of these penetrate to about the 100-hPa level. There is an extensive layer of anvil cloud at upper levels and a neutrally stable layer from about 250 to 170 hPa. This layer is apparently destabilized due to radiative cooling at cloud top. A plot is shown in Fig. 2 of the vertical velocity for an east–west vertical cross section (8°S) through the 3-km mesh grid at about tau = 8 h. The two largest cells shown here eventually reached the tropopause. The modest vertical velocities simulated are consistent with observations of tropical oceanic convection reported by LeMone and Zipser (1980) and Zipser and LeMone (1980), but weaker than the strong updrafts (17 m s^{-1}) observed in the tropical Pacific (South China Sea) during the Winter Monsoon Experiment (WMONEX; Churchill and Houze 1984). One concern is the impact of the coarse horizontal resolution

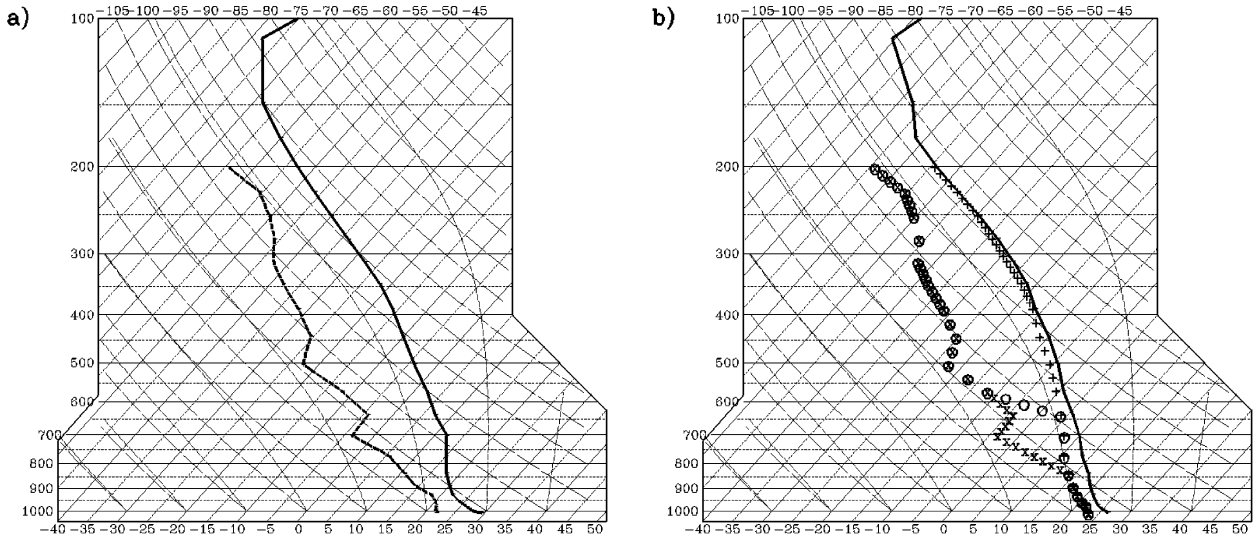

FIG. 3. Skew *T*–log *p* diagrams for (a) TOGA COARE IFA region at 0000 UTC, 14 Nov 1992; (b) mean lateral boundary conditions during Forecasts A, B, and C. The solid line is the temperature profile. Dewpoint temperatures are plotted with (+) for Forecast A, (○) for Forecast B, and (×) for Forecast C. Pressure is given (in hPa) on the left axis, and temperature (in °C) on the bottom.

that is used. In this regard, note that Weisman et al. (1997) found evidence that 4-km horizontal resolution was sufficient to reproduce momentum and heat transports of midlatitude squall-line-type convective systems. It is not clear to what extent the same would hold for the tropical Pacific convection modeled here. Although the horizontal grid-dimension sensitivity was not tested, as discussed in section 4, it appears that such sensitivity would not alter the main conclusions of this study.

In order to investigate the effect of dry layers above the boundary layer on the simulated convection, a series of additional 24-h forecasts were carried out. To prepare for the first three additional forecasts, the update cycle used for Forecast CTL was modified for 24 h beginning at 0000 UTC on 20 November by changing the lateral moisture boundary conditions. The modified boundary conditions were identical to those for the corresponding spinup for Forecast CTL below 800 hPa, but above this level a dry TOGA COARE moisture profile (an average over the IFA region from 0000 UTC on 14 November 1992) was used (Ciesielski et al. 1997). The water vapor mixing ratio was initialized to the TOGA COARE profile above 800 hPa at the beginning of this period. The three additional forecasts that were started 24 h later (0000 UTC on 21 November 1998) thus began with a dry sounding at mid to upper levels. Of these three forecasts, the one that will be referred to here as Forecast A was carried out using lateral moisture boundary conditions for the 3-km mesh grid obtained from the parent 9-km mesh grid. In the second forecast, Forecast B, the lateral moisture boundary conditions were the same as for Forecast A below 600 hPa, but were set to the values from the TOGA COARE moisture profile above that level. In the third forecast, Forecast C, the moisture boundary conditions were treated the same as for Forecast B, except the threshold pressure level was changed from 600 to 800 hPa. The three forecasts thus differ only insofar as the differences in the moisture advected into the 3-km mesh grid. Soundings are shown in Fig. 3 that illustrate the extent of these differences. The sounding corresponding to the dry TOGA COARE moisture profile that was used is shown in Fig. 3a. The soundings in Fig. 3b show the mean lateral boundary conditions for the 3-km mesh grid during Forecasts A, B, and C. It is clear from the sounding for Forecast A that the 3-km mesh is embedded in a very moist environment during these forecasts, particularly so at upper levels. The TOGA COARE sounding shown in Fig. 3a is quite dry by contrast, so the lateral moisture boundary conditions in Forecasts B and C are much drier than in Forecast A above their respective pressure thresholds of 600 and 800 hPa. These forecast experiments, as well as other simulations described here, are summarized in Table 1.

Results for Forecasts A, B, and C are shown in Fig. 4 for the simulated ''3-km mesh-mean'' mixing ratio of precipitating hydrometeors as it varied with forecast time. In these and subsequent plots, the plotted mean results represent a 72 × 72 gridpoint subdomain of the entire 3-km mesh grid to ensure adequate removal from the boundaries. The results shown in Fig. 4a for Forecast A are very similar to those for Forecast CTL (not shown), though with somewhat less precipitation. The simulated peak cloud-top heights are not significantly affected by the dry layer that is maintained in Forecasts B and C, though these forecasts have substantially less precipitating condensate than Forecast A. The surface precipitation, for example, in Forecast B is 37% less than for Forecast A. This precipitation sensitivity is con-

TABLE 1. Summary of moisture sensitivity forecast experiments.

Experiment	Description
Forecast CTL	Control
Forecast A	Same as CTL, but forecast is preceded by a 24-h spinup period during which a dry layer is imposed on the COAMPS 3-km mesh grid.
Forecast B	Same as A, but dry lateral boundary conditions above 600 hPa.
Forecast C	Same as A, but dry lateral boundary conditions above 800 hPa.
Forecast D	Same as A, but dry lateral boundary conditions between 800 and 600 hPa.
Forecast E	Same as A, but dry lateral boundary conditions between 600 and 400 hPa.
Forecast F	Same as A, but dry lateral boundary conditions between 400 and 200 hPa.

sistent qualitatively with TOGA COARE observations of the relationship between dry layers at mid to upper levels and rainfall. Rainfall in Forecast C is even further reduced.

Although large differences in the lateral boundary conditions for the experimental forecasts are evident in Fig. 3, it is important to verify the impact of these differences on the COAMPS 3-km mesh grid moisture field during the forecasts. Plots in Fig. 5 show the 3-km mesh-mean sounding at tau = 0, and also at tau = 5 h for Forecasts A, B, and C. The soundings show that, by 5 h into the forecasts, the moisture differences are significant and generally in agreement with what one would expect based on the differences in lateral boundary conditions. One exception is that above about 270 hPa the soundings are very moist, perhaps due to moisture trans-

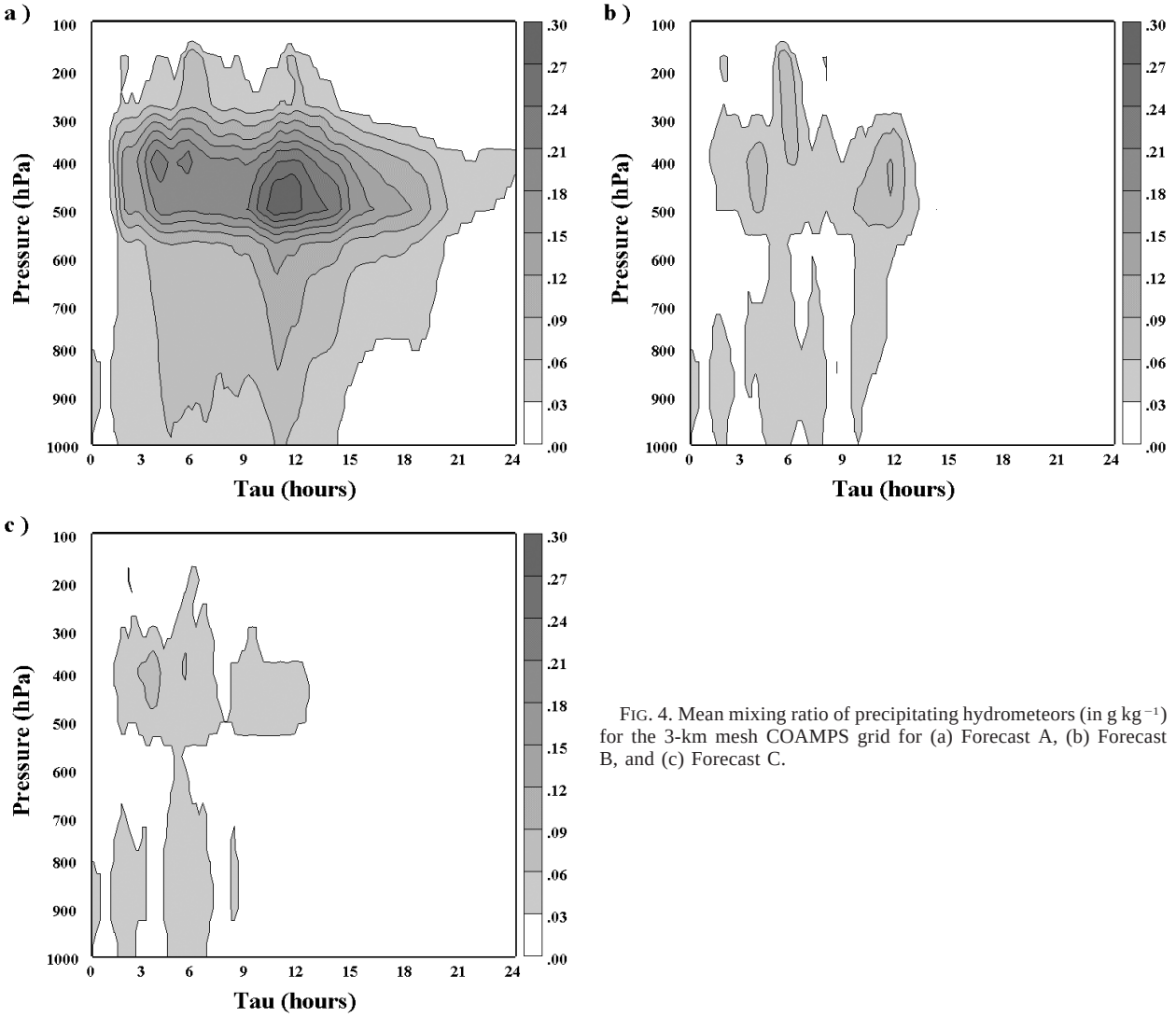

FIG. 4. Mean mixing ratio of precipitating hydrometeors (in g kg^{-1}) for the 3-km mesh COAMPS grid for (a) Forecast A, (b) Forecast B, and (c) Forecast C.

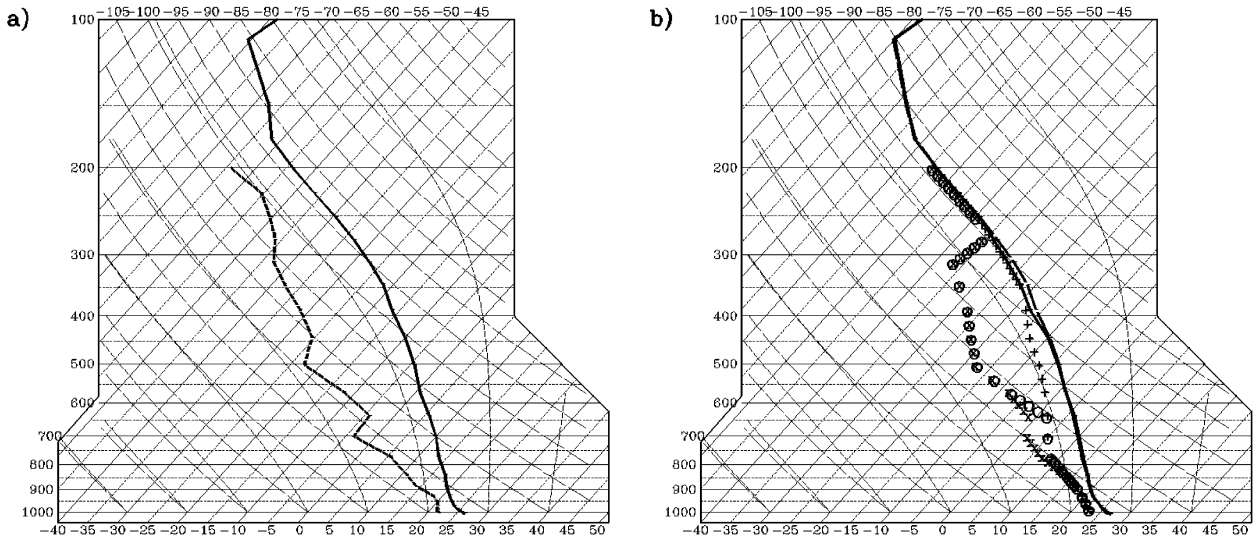

FIG. 5. Skew T–log p diagrams for COAMPS 3-km mesh grid for Forecasts A, B, and C at (a) tau = 0; (b) tau = 5 h. In (b), the dashed line is the temperature profile for Forecasts A, and the solid line is the temperature profile for Forecasts B and C. Dewpoint temperatures in (b) are plotted with (+) for Forecast A, (○) for Forecast B, and (×) for Forecast C. Pressure is given (in hPa) on the left axis, and temperature (in °C) on the bottom.

port associated with convection. The moisture profiles at tau = 10 h (not shown) differ in some respects from those at tau = 5 h, but retain the essential features noted here. Of particular relevance is the fact that the soundings at low levels in Forecasts A and B are comparably moist, supporting the conclusion that enhanced dryness at mid to upper levels is responsible for the reduced precipitation obtained in Forecast B with respect to Forecast A. In related experiments, Tompkins (2001) found that decreased moisture above 700 hPa led to what for the most part was a gradual reduction of rainfall (on the order of days) compared with the sudden reduction obtained by extending the moisture perturbation down to 900 hPa. The slower timescale associated with the impact of the upper-level moisture perturbation could be attributed to the time required for subsidence to bring the dry moisture perturbation to the lower troposphere. The current results cannot be explained in this manner. One possible explanation for the difference is the importance of wind shear for enhancing mixing with the environment. The aforementioned experiments of Tompkins (2001) were carried out with no imposed winds, and hence presumably for a generally weakly sheared environment. In comparison, the shear in the present forecasts was fairly substantial. To illustrate, the 3-km mesh-mean wind profile at the start of Forecasts A, B, and C is shown in Fig. 6. The vertical shear at mid to upper levels in particular is significant, and can be expected to enhance mixing of environmental air with updrafts compared with a low-shear environment. Other possible factors relating to the different moisture sensitivities reported here versus previous studies are discussed in section 2d below.

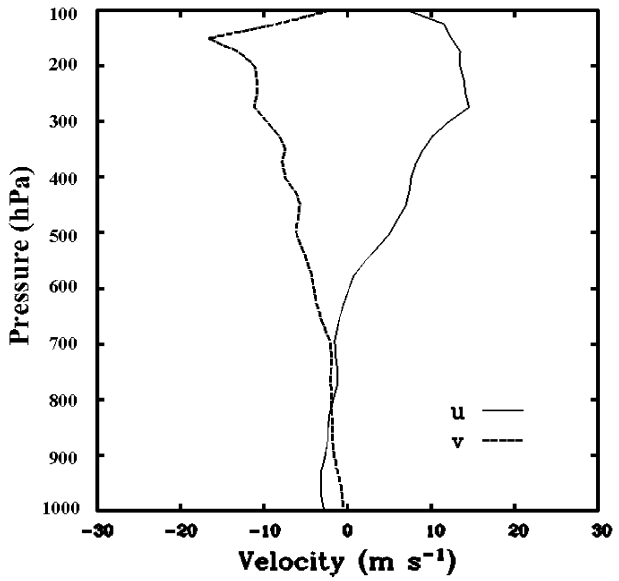

FIG. 6. Wind components u and v (in m s^{-1}) at tau = 0 for Forecasts A, B, and C.

In order to clarify the implications of the preceding experiments additional tests were performed. Forecasts D, E, and F were carried out in a similar manner as Forecasts A, B, and C, but with the following differences. In Forecast D, the dry lateral boundary conditions were imposed only in a layer between 800–600 hPa. Forecasts E and F were similar in design, but with the dry layer between 600–400 hPa and 400–200 hPa, respectively, in these forecasts. The 3-km mesh-mean precipitating hydrometeor mixing ratios are plotted in Fig. 7. The dry layer has a considerable impact in all three cases (comparing with Forecast A), but is particularly

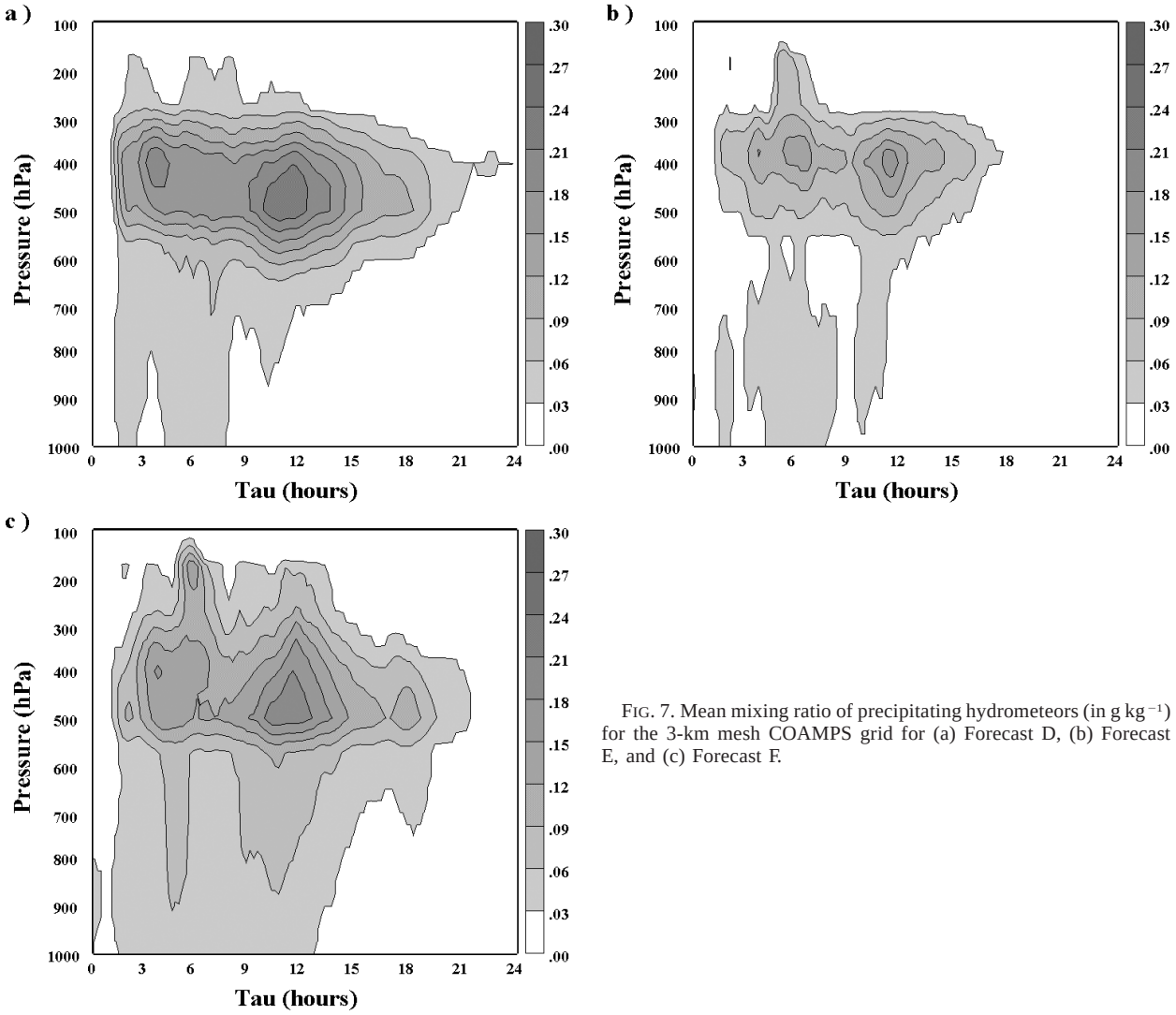

FIG. 7. Mean mixing ratio of precipitating hydrometeors (in g kg^{-1}) for the 3-km mesh COAMPS grid for (a) Forecast D, (b) Forecast E, and (c) Forecast F.

large for Forecasts D and E. Comparing the latter two forecasts, one finds that dry air at mid levels has a greater impact in reducing the amount of precipitating hydrometeors at mid levels than does dry air at low levels. Dry air at low levels, nonetheless, has a considerable impact in enhancing the evaporation of precipitation before it reaches the surface.

c. Precipitation production sensitivity

The physical interpretation of the results, suggested by the preliminary discussion in section 1, is that the simulated convection is inhibited in the presence of dry air aloft due to the impact of entrainment of the dry air into the updrafts. This view requires verification, especially in light of the fact that horizontal turbulent mixing is not treated in the present COAMPS simulations. One could suppose, for example, that precipitation formed within simulated updrafts is evaporated to a greater degree in the dry layer simulations upon being detrained, or upon falling out of the updrafts (cf. Emanuel and Zivkovic-Rothman 1999). In order to investigate this point, the simulations were rerun while outputting the mixing ratio tendency due to phase changes for precipitating hydrometeors. The mean value of the maximum of this quantity and zero over the model domain is a measure of the amount of precipitation that is formed. The results obtained are shown in Fig. 8a for Forecast A and Fig. 8b for Forecast B. There is a considerable difference between the two plots. Note that Forecast A has a substantial amount of precipitation formation at mid levels due to cold rain processes. This feature appears to be an important factor in the precipitation sensitivity to dry layers at mid to upper levels shown in Figs. 4 and 7. In contrast, Forecast B has much less precipitation production at mid levels. Because precipitation forms within clouds, the implication is that precipitation is reduced in Forecast B due to the mixing

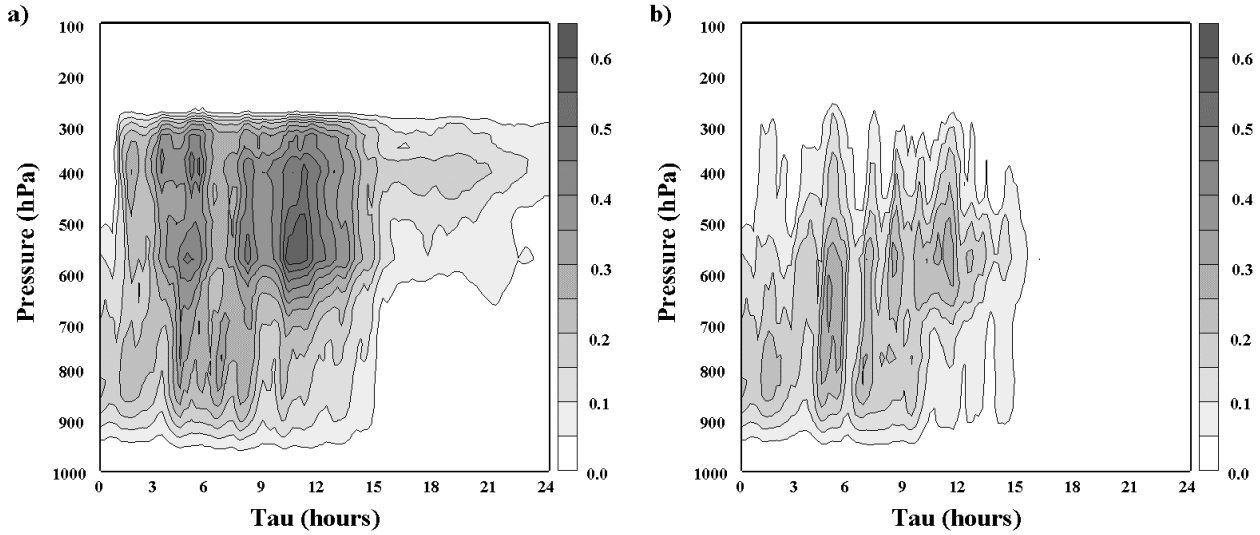

FIG. 8. Mean of the maximum value of zero and the precipitation production rate (in g kg^{-1} h^{-1}) for the 3-km mesh COAMPS grid for (a) Forecast A; (b) Forecast B.

of dry environmental air into the updrafts. This process is represented by the buoyancy sorting model of Raymond and Blyth (1986) that is implemented in the convective parameterizations of Emanuel (Emanuel 1991; Emanuel and Zivkovic-Rothman 1999) and Kain and Fritsch (1990). The present simulations may thus provide a useful test for these parameterizations, and the comparative performance of these schemes is investigated in section 3 below.

d. Previous studies and further tests

The significant sensitivity to midlevel moisture noted here contrasts somewhat with other modeling studies that have been reported (e.g., Lucas et al. 2000; Tompkins 2001). In the case of the Tompkins study, the potential significance of the low shear environment has already been addressed in the preceding discussion. Another factor to be considered is that such differences can be expected to depend considerably on the nature of the moisture perturbations that are tested. Previous studies did not examine the impact of imposing dry layer perturbations based on observed variability associated with tropical dry tongue episodes. During TOGA COARE, moisture variability associated with the occurrence of major dry events was greatest at upper levels. Brown and Zhang (1997) reported mixing ratio decreases during dry events of about 6% with respect to mean values between the surface and 950 hPa, and 67% between 550–200 hPa. Lucas et al. (2000) and Tompkins (2001) both used height-invariant moisture perturbations in layers where perturbations were applied, and it is reasonable to expect that the results may not be representative of the relative importance of mid- to upper-level moisture variability associated with the dry tongue phenomenon. Another potentially important feature in moisture sensitivity investigations concerns the level at which precipitation production is greatest. This point was briefly mentioned in the preceding section. If rain is predominantly formed by warm rain processes, then mid- to upper-level dry layers may have a muted effect on convective rainfall. The significant role of cold rain processes in Forecast A may partly explain the importance of mid- to upper-level moisture in the present study.

It should be emphasized that the present results are not inconsistent with a significant sensitivity of convection to low-level moisture variations associated with dry tongues. This is evident, for example, from the results for Forecast D shown in Fig. 7a. Furthermore, experiments using a TOGA COARE moisture profile (13 November 1992 IFA mean at 0600 UTC) that is significantly drier between 800–700 hPa than the profile used here yield a somewhat more pronounced effect to maintaining the perturbation down to 800 hPa, in particular a greater cloud-top-height sensitivity. For this case as well, however, there is a considerable sensitivity of the rainfall to the moisture above 600 hPa.

3. Convective parameterization tests

a. Method

The COAMPS experiments described in the preceding section provide evidence for a considerable sensitivity of deep convection to moisture variability both at mid to upper levels and at low levels of the nature associated with the tropical dry tongue phenomenon. In the present section the behavior of parameterized convection with respect to the moisture variability explored in Forecasts A and B at mid to upper levels is investigated. In order to assess the behavior of parameterized

convection in a column mode for these cases, data was output from COAMPS during the forecasts that can be used to run COAMPS as an SPM or an SCM. Data was output every 6 min from the COAMPS 3-km grid, including advective tendencies, atmospheric profile data, radiative heating profiles, and surface fluxes. The saved data are all time-averaged over the 6-min intervals, except for the atmospheric profile data. In the column model tests, in order to help reduce the dependence of the results on particular features of COAMPS, the surface fluxes and radiative heating rates (atmospheric as well as surface) were taken to be the same as those predicted on the COAMPS 3-km mesh grid.

The SPM and SCM convective parameterization tests require appropriate advective tendency data from the 3-km mesh COAMPS forecasts over selected domains. To this end, horizontal advective tendencies of potential temperature and moisture variables are simply averaged across the selected test domains. Using subscript H to denote the resultant horizontal advective tendencies,

$$\left(\frac{\partial q}{\partial t}\right)_H = \overline{\left(-u\frac{\partial q}{\partial x} - v\frac{\partial q}{\partial y}\right)}, \tag{1}$$

where q denotes mixing ratio or potential temperature, u and v represent the horizontal wind components, and the overbar denotes averaging over a selected domain. In computing the vertical advective tendencies for the column model tests, it is important to bear in mind that vertical motions on the scale of the 3-km mesh grid accomplish the vertical mixing that cumulus parameterizations are designed to represent for coarser grids. To simply use the average of the 3-km mesh grid vertical advective tendencies over the selected test domains would therefore not be appropriate. A quantity representing the contribution of small-scale (in this case the 3-km mesh grid scale) vertical motions is thus subtracted from the area-mean vertical advective tendencies. Using subscript V to denote the resultant (large scale) vertical advective tendencies, one obtains

$$\left(\frac{\partial q}{\partial t}\right)_V = \overline{-w\frac{\partial q}{\partial z}} - \overline{\left(-\frac{1}{\rho}\frac{\partial(\rho q' w')}{\partial z}\right)}, \tag{2}$$

where w is vertical velocity, ρ is density, and primes denote deviations from the area mean. The mass-weighted vertical integral of the small-scale mixing term in (2) is approximately equal to zero as long as the vertical velocity is small at the surface (or vanishes there as in the present study).

Advective tendencies and pressure gradient force contributions to the wind components are simply averaged across the selected test domains, time-averaged, and saved to files during the COAMPS forecasts. In the SCM runs for the present work, the wind fields are for the most part simply maintained at the area-averaged values over the test domains as in the SPM runs, but the saved tendencies are used to adjust the wind field values during 6-min intervals between model calls to read in the 3-km mesh grid COAMPS data. The pressure variable is treated in an analogous manner.

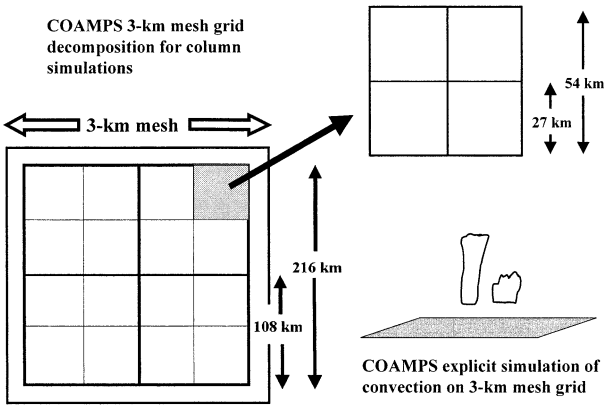

FIG. 9. Model grid framework for the SCM and SPM experiments.

The advective tendencies and area-averaged atmospheric profiles, radiative heating profiles and surface fluxes are output for overlapping domains of varying size as illustrated in Fig. 9. The figure illustrates the decomposition of the COAMPS 3-km mesh grid into square regions or ''boxes'' with sides of length varying from 27 to 216 km. By running the SPM and SCM for each of these boxes and averaging results for equal-sized boxes, one obtains results showing the performance of a given convective scheme as it varies with grid dimension. This feature is significant because the performance of convective parameterizations can be expected to depend on the horizontal grid resolution. This is true for example of buoyancy-sorting-based schemes which require information on the local cloud environment, and hence are probably best suited for relatively high-resolution grids of ~30 km or less (cf. Kain and Fritsch 1990). Available observational datasets suitable for SCM testing generally represent fairly large regions, on the order of several hundred kilometers, and may not be suitable for testing of such schemes. The present framework is well-suited to exploring this point.

b. Semiprognostic tests—Rainfall

The SPM tests provide a picture of how the convective parameterizations would perform in an otherwise perfect model forecast. When the parameterizations are used for numerical weather prediction or in SCM forecasts, error is introduced in part due to imperfections in the parameterized physics. Rainfall is used here as the primary measure of the SPM performance, and errors in the SPM rainfall forecasts give one indication of the extent to which model forecasts will suffer due to the performance of the convective schemes.

Semiprognostic simulations were carried out using the data output from Forecasts A and B of section 2. Simulations were performed using both the Emanuel

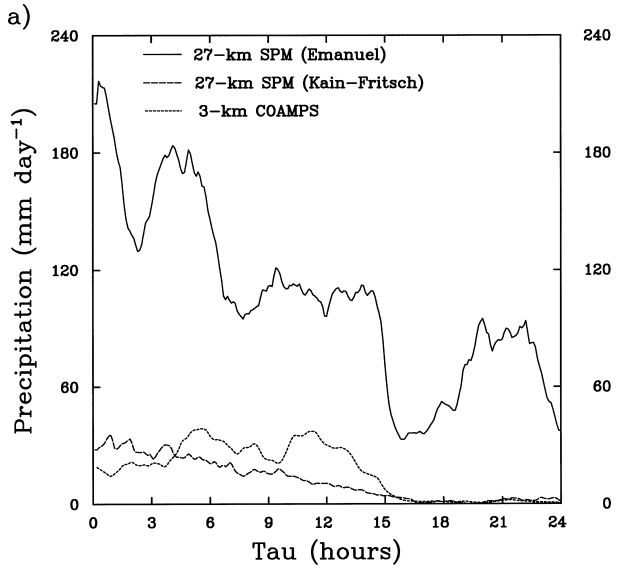

FIG. 10. Precipitation (in mm day^{-1}) obtained with the Emanuel and Kain–Fritsch convective schemes in 27-km-resolution SPM forecasts for Forecast A. Corresponding results from the COAMPS 3-km mesh grid in Forecast A are also shown.

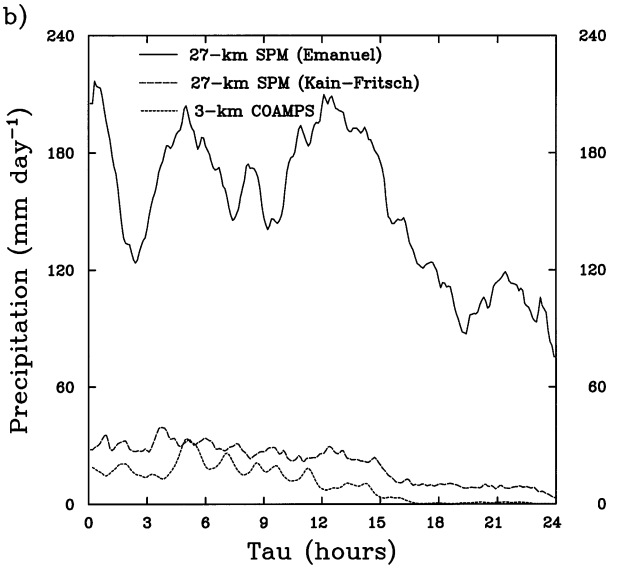

FIG. 11. Precipitation (in mm day^{-1}) obtained with the Emanuel and Kain–Fritsch convective schemes in 27-km-resolution SPM forecasts for Forecast B. Corresponding results from the COAMPS 3-km mesh grid in Forecast B are also shown.

convective parameterization and the Kain–Fritsch convective parameterization. The precipitation predicted directly by the convective parameterizations in the SPM simulations was compared with the precipitation predicted by COAMPS on the 3-km mesh grid. To the extent that the 3-km mesh grid rainfall is of convective origin, this is the appropriate comparison to make. Explicitly simulated rainfall in the SPM simulations is due to rainwater introduced into the SPM grid directly from the COAMPS 3-km mesh grid. Assuming this rainwater is of convective origin, its contribution to the surface precipitation would produce a positive bias in the rainfall for a perfectly functioning convective scheme. Where the convective parameterizations appear to underpredict the rainfall, an assessment must be made as to the degree to which the 3-km mesh rainfall is indeed of convective origin.

Convective rainfall rates from the 27-km-resolution semiprognostic tests are plotted in Fig. 10 (Forecast A) and Fig. 11 (forecast B) as a function of forecast time. The rainfall predicted explicitly on the 3-km mesh COAMPS grid in Forecasts A and B is also plotted. The results obtained from the convective parameterizations are mixed. The Emanuel scheme overpredicts the precipitation by a considerable amount. Whereas the amount of precipitation for Forecasts A and B was 16.7 and 10.6 mm, respectively, the Emanuel scheme gives corresponding values of 105.9 and 152.1 mm for the amount of convective precipitation. The Kain–Fritsch scheme does better in these tests than does the Emanuel scheme, with convective rainfall totals considerably closer to rainfall amounts predicted on the COAMPS 3-km mesh grid. The rainfall totals are summarized in Table 2 for the 27-km-resolution semiprognostic runs. Results from separate tests (not shown) show that the very excessive rainfall predicted by the Emanuel scheme is due to its sensitivity to a specified temperature deficit at cloud base in the cloud-base mass flux parameterization (Emanuel and Zivkovic-Rothman 1999).

Note that both the Emanuel and Kain–Fritsch schemes fail to adequately account for the impact of the drier sounding in forecast B. Whereas the COAMPS 3-km mesh grid shows a 37% reduction in rainfall in Forecast B with respect to forecast A, the convective parameterization results show greater convective rainfall for Forecast B than for Forecast A. This result is somewhat unexpected. Both of the convective parameterizations used here employ a buoyancy-sorting scheme to predict convective mass flux profiles that can be expected to account to some extent for the impact of environmental moisture variations aloft on convection (cf. Kain and Fritsch 1990). Some insight into the failure of the convective schemes to predict less rainfall for Forecast B than for Forecast A can be obtained by noting that, although the experiment was designed to examine the

TABLE 2. Rainfall totals from the COAMPS 3-km mesh and 27-km SPM forecasts (in mm).

	COAMPS 3D forecast		Emanuel SPM forecast		Kain–Fritsch SPM forecast	
Rainfall (mm)	A	B	A	B	A	B
Total	16.7	10.6	119.8	160.3	26.0	29.1
Convective			105.9	152.1	12.2	21.0
Grid scale			13.9	8.2	13.8	8.1

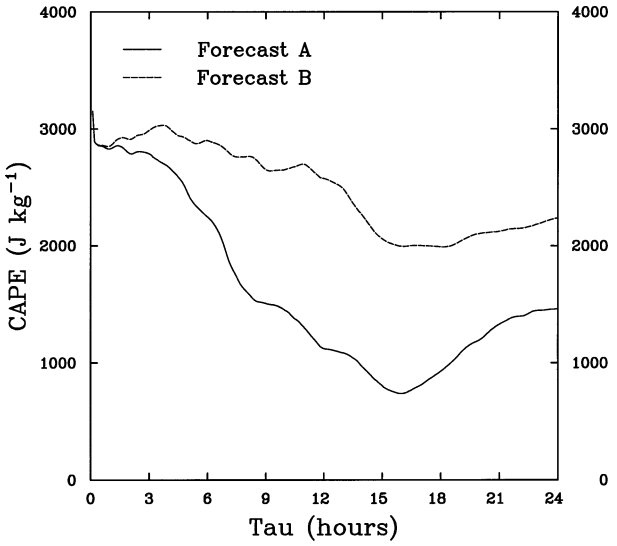

FIG. 12. CAPE (in J kg^{-1}) in Forecasts A and B.

impact of dry air above the source layer on convection, the decrease in convection in Forecast B has the effect of maintaining a higher amount of buoyant energy in the atmosphere. This fact is evident in the plots of convective available potential energy (CAPE; e.g., Emanuel 1994) in Fig. 12. Both the Kain–Fritsch scheme and the Emanuel scheme compute cloud-base mass fluxes in a manner that results in larger mass fluxes and convective rainfall under conditions of greater parcel buoyancy (at cloud base and below, in the case of the Emanuel scheme). Plots of cloud-base mass flux predicted by the two schemes in Fig. 13 indeed show larger values for the drier case (Forecast B). It is helpful to compare the cloud-base mass fluxes in Fig. 13 with vertical mass fluxes on the COAMPS 3-km mesh grid. In order to filter out the contribution of large-scale uplift, the 3-km mesh vertical velocities were first processed by subtracting from the value at each point the local 27-km box mean vertical velocity (corresponding to the subdomains illustrated in Fig. 9). The resultant values that did not exceed a vertical velocity of 1 m s^{-1} were set to zero in order to compute only the ''updraft core'' vertical mass fluxes, and filter out the contribution of smaller-scale eddies. The results are plotted in Fig. 14. In general, the low-level vertical mass fluxes appear to be at least somewhat larger for Forecast A than Forecast B. At 900 hPa, for example, the mean value for Forecast A exceeds that of Forecast B by 13%. This result stands in contrast with the parameterized results shown in Fig. 13. Note that the temporal evolution of the vertical mass fluxes in Fig. 14 more closely follows that seen in Fig. 13b for the Kain–Fritsch scheme.

c. Semiprognostic tests—Resolution sensitivity

The buoyancy-sorting model implemented in the convective parameterizations tested here is expected to have some sensitivity to the horizontal resolution. Other aspects of the parameterizations, such as the closure treatments, can be expected to exhibit scale dependence as well. Though such scale dependence is not unexpected, its magnitude is generally not known. It may be helpful therefore to briefly look at this point, which is readily assessable via the present testing framework. To this end, plots of convective rainfall from the 108- and 216-km Emanuel and Kain–Fritsch SPM tests for Forecast A are shown in Fig. 15. These plots can be compared

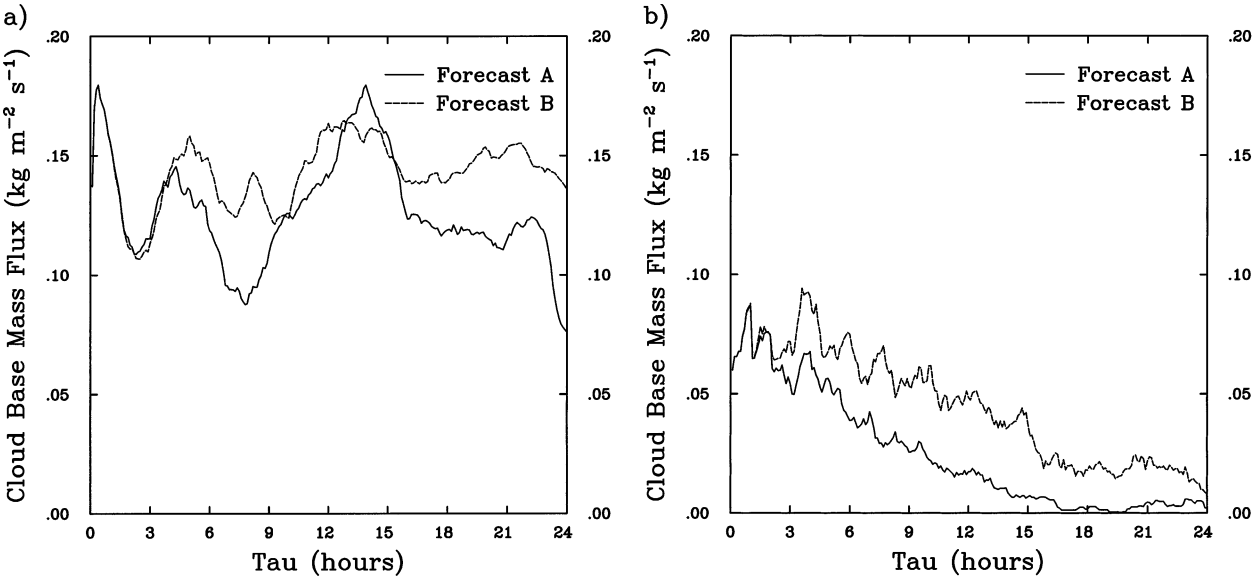

FIG. 13. Cloud-base mass flux (in kg m^{-2} s^{-1}) in the 27-km-resolution SPM forecasts corresponding to Forecasts A and B using (a) the Emanuel convective scheme; (b) the Kain–Fritsch convective scheme.

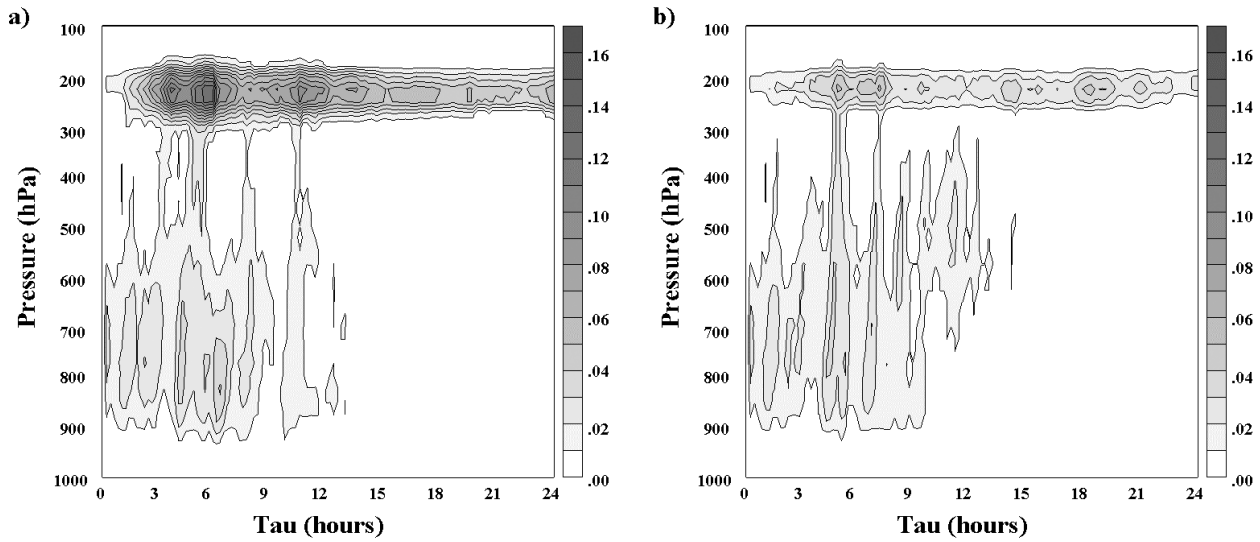

FIG. 14. Updraft core vertical mass flux (in kg m^{-2} s^{-1}) in (a) Forecast A; (b) Forecast B.

with the corresponding 27-km results shown in Fig. 10. There are substantial differences in the temporal evolution of the parameterized rainfall at the different resolutions, with greater amounts of convective precipitation occurring at the 27-km resolution. The scale sensitivity for the Kain–Fritsch scheme in this case appears to be considerably less than that for the Emanuel scheme, at least for scales less than 108 km. At 216-km resolution, the results of both parameterizations differ considerably from the respective 27-km results. Note that convective precipitation ceases at about tau = 7 h in the 216-km resolution tests, even though there is at that time still heavy precipitation on the 3-km mesh grid. The cessation is brief in the case of the Emanuel scheme, but convective rainfall does not resume with the Kain–Fritsch scheme for the remainder of the forecast. As indicated above, an apparent deficiency in parameterized convective rainfall could merely reflect the fact that the rainfall on the 3-km COAMPS grid was not of convective origin. A simple means to assess the extent to which there is a significant amount of convective rainfall after tau = 7 h is to look at plots of the surface rainfall rate for forecast A. Cellular distributions of precipitation at tau = 8 h (Fig. 16a) and tau = 12 h (Fig. 16b) clearly show a large proportion of convective rainfall at both times. Evidence for continued deep convection subse-

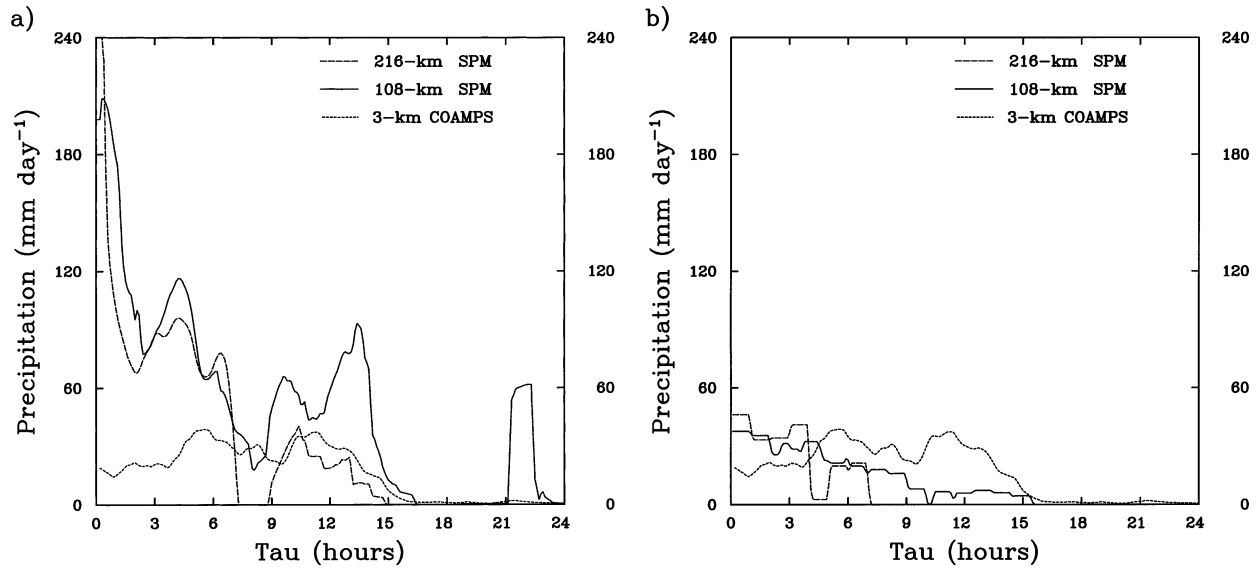

FIG. 15. Precipitation (in mm day^{-1}) obtained in 108- and 216-km-resolution SPM forecasts corresponding to Forecast A with (a) the Emanuel convective scheme; (b) the Kain–Fritsch convective scheme. Corresponding results from the COAMPS 3-km mesh grid in Forecast A are also shown.

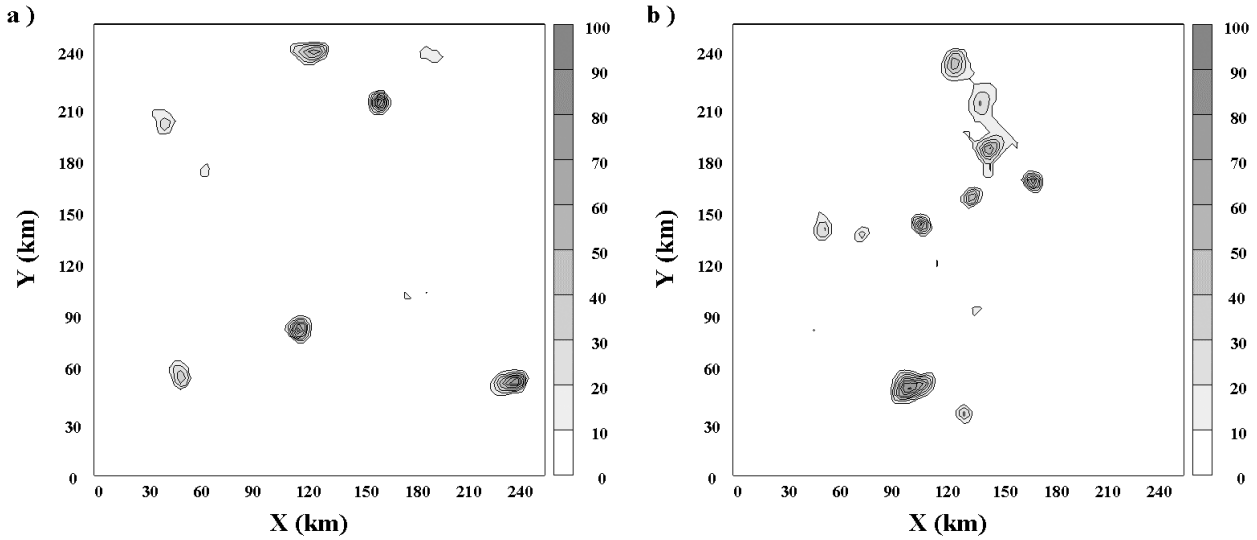

FIG. 16. Surface rainfall rate (in mm h^{-1}) over the COAMPS 3-km mesh grid domain for Forecast A at (a) tau = 8 h; (b) tau = 12 h.

quent to tau = 7 h in Forecast A is also found in the updraft mass flux profile plotted in Fig. 14a. There is evidence therefore to support the conclusion that the 216-km resolution was too coarse for the Kain–Fritsch parameterization to represent the later stages of the convective episode in Forecast A. The convective parameterizations exhibit considerable horizontal-scale sensitivity for Forecast B as well (not shown). In this case, the difference between the 108- and the 27-km SPM results for the Kain–Fritsch scheme is greater than that obtained for Forecast A, apparently a reflection of the drier large-scale environment at mid to upper levels in this forecast.

d. Semiprognostic tests—Parameterized mass flux profiles

One means of diagnosing the effectiveness of the buoyancy-sorting updraft/environment mixing implementations in the Emanuel and Kain–Fritsch parameterizations is to compare the predicted total updraft mass flux profiles with the results plotted in Fig. 14 for the corresponding COAMPS forecasts. Updraft mass flux profiles have been used for diagnostic purposes for example by Kain and Fritsch (1990) and Lucas et al. (2000). The total updraft mass flux is plotted in Fig. 17 for the Emanuel scheme, and in Fig. 18 for the Kain–Fritsch scheme. If one ignores the large mass fluxes

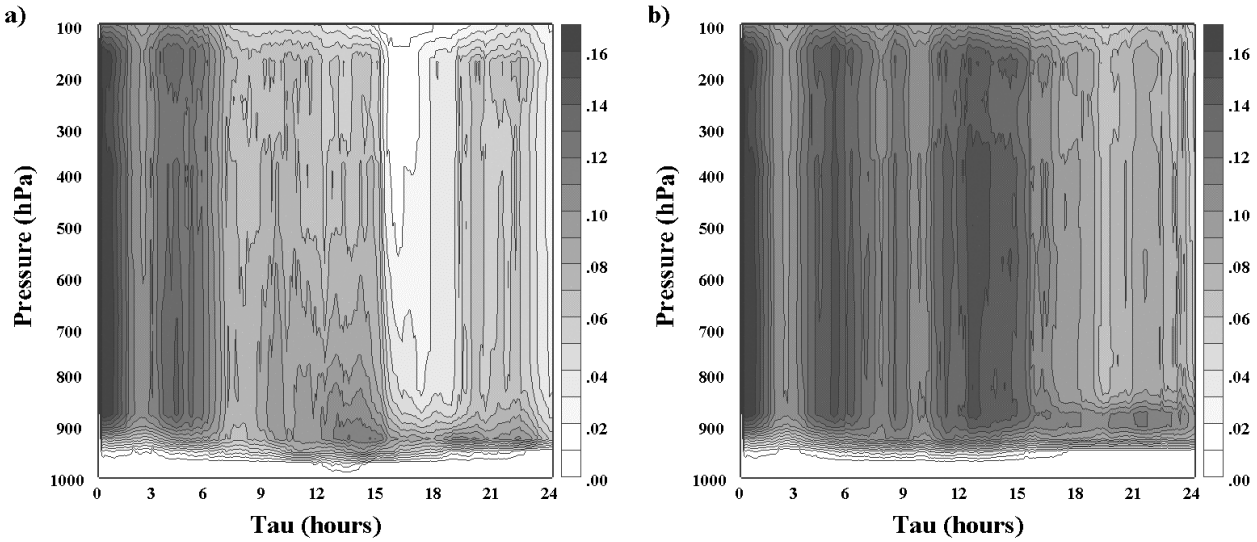

FIG. 17. Updraft mass flux (in kg m^{-2} s^{-1}) for the 27-km-resolution Emanuel SPM tests for (a) Forecast A; (b) Forecast B.

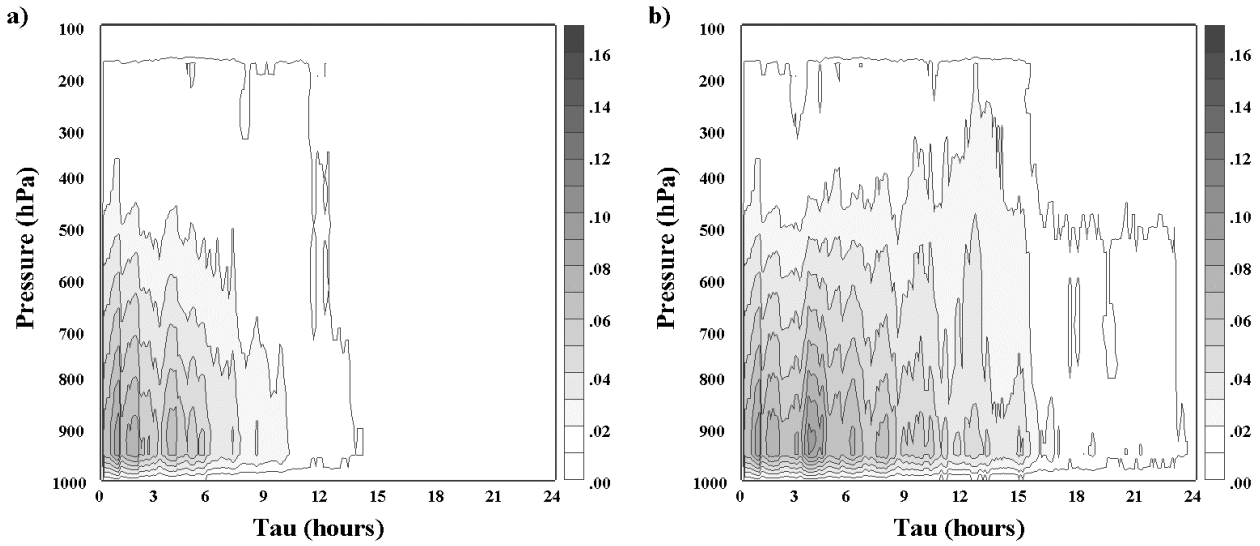

FIG. 18. Updraft mass flux (in kg m^{-2} s^{-1}) for the 27-km-resolution Kain–Fritsch SPM tests for (a) Forecast A and (b) Forecast B.

associated with circulations near the tropopause (Fig. 2) in the COAMPS forecasts, the profiles obtained in the SPM tests with the Kain–Fritsch parameterization appear reasonable to some degree. However, the amount of net detrainment at mid levels appears to be somewhat excessive compared with the COAMPS forecasts. The updraft mass fluxes from the Emanuel scheme are too large and, except for a period near the middle of Forecast A, they do not show evidence of the substantial net detrainment at mid levels apparent in the COAMPS and Kain–Fritsch results. The lesser amount of detrainment with the Emanuel scheme may reflect its explicit allowance for undilute air from the source level to mix with the environment throughout the depth of the cloud, resulting in a greater tendency for buoyant mixtures of cloudy and environmental air in the buoyancy-sorting treatment.

Care must be taken in assessing the updraft mass flux data. One must remember, for example, that the vertical mass fluxes shown in Fig. 14 for COAMPS only represent the updraft cores as defined above. Corresponding plots (not shown) with the vertical velocity threshold set to zero (rather than 1 m s^{-1}) show updraft roots extending very close to the surface, in better agreement with the parameterized results. It should also be noted that in the computation of the updraft mass flux for the Emanuel scheme, the negative contributions of parcel mixtures that descend to detrain at lower levels are included (Emanuel 1991). There is some uncertainty whether the results shown are strictly comparable with the results plotted for COAMPS (Fig. 14) and the Kain–Fritsch SPM forecast (Fig. 18), because such negative contributions have not been accounted for in these cases. However, a test of the sensitivity to neglecting the descending drafts in the Emanuel scheme was carried out for Forecast A, and virtually no impact was observed.

e. Single-column model tests

The SPM forecasts have as a strength the fact that they allow one to run parameterizations under specified atmospheric conditions. From the perspective of a mode of testing parameterizations, it can be difficult to ascertain the extent of the bias one might expect in actual forecasts because there is no feedback from the model physics to the atmospheric profile. This bias can be investigated through SCM experiments, which allow for some degree of model feedback. For the present work, SCM tests analogous to the SPM tests discussed above were thus carried out. One weakness of SCM forecasts is that the advective tendencies are simply prescribed, and do not depend on the details of the SCM forecast. This feature, however, can also be beneficial by helping to constrain the column model, and by facilitating model diagnostics.

SCM forecasts were carried out corresponding to each of the semiprognostic tests for Forecasts A and B discussed in the preceding sections. The 27-km-resolution precipitation results are illustrated in Fig. 19 (Forecast A) and Fig. 20 (Forecast B), and summarized in Table 3. Whereas, for the semiprognostic tests, it was appropriate to focus on the convective precipitation, the total precipitation is plotted here as well since there is no danger of double counting. The results for the Emanuel scheme contrast considerably with the SPM results in Figs. 10 and 11, and in Table 2, with precipitation rates generally much closer to the COAMPS 3-km rainfall. Note that there appears to be an excessive amount of grid-scale rainfall for Forecast A, particularly with the Kain–Fritsch scheme.

The excessive rainfall evidenced in the SPM results for the Emanuel scheme is reflected in the excessive rainfall rates for the initial 30 min or so in the plots in

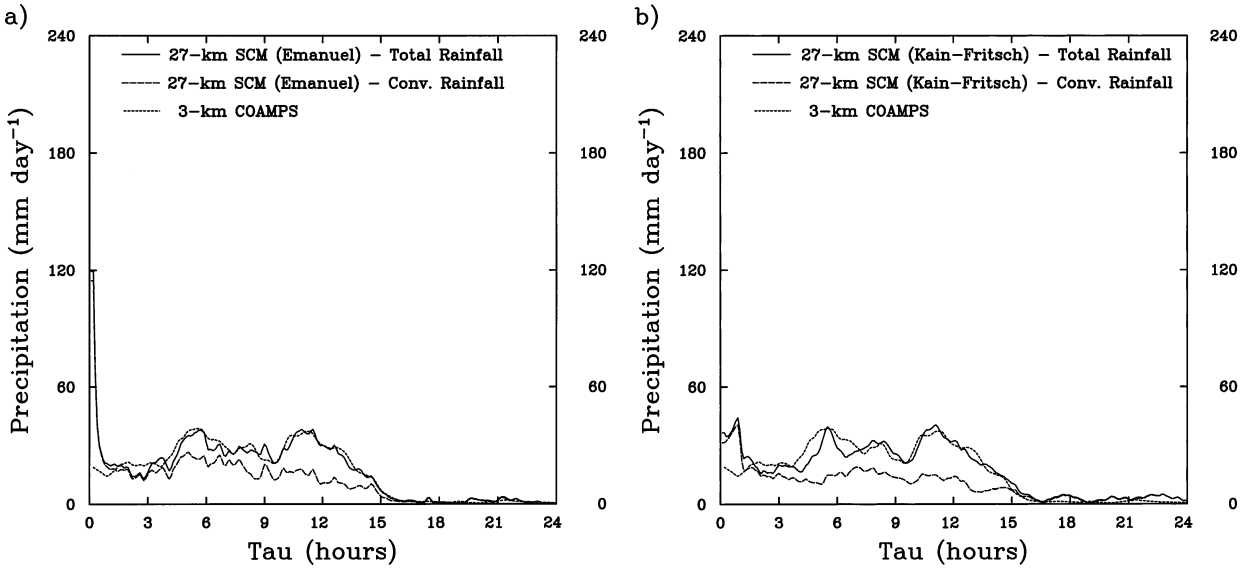

FIG. 19. Precipitation (in mm day^{-1}) obtained in 27-km-resolution SCM forecasts for Forecast A with the convective schemes of (a) Emanuel and (b) Kain–Fritsch. Corresponding results from the COAMPS 3-km mesh grid in Forecast A are also shown.

Figs. 19 and 20. Various measures of the bias introduced during this spinup period, as well as during the remainder of the forecasts, can be investigated. For example, in light of the discussion above concerning the dependence of the convective parameterizations on parcel buoyancy, it is pertinent to examine how the CAPE evolves during the SCM forecasts. This quantity is plotted in Fig. 21 for the 27-km-resolution SCM forecasts, as well as for the COAMPS 3-km mesh grid in Forecasts A and B (computed as a mean of 27-km-resolution values). One sees that the initial excessive rainfall produced by the Emanuel scheme results in a substantial reduction in CAPE to values well below those obtained in the COAMPS forecasts. In general, the errors are large and consistent with the indications from the SPM experiments that the convective schemes tested here cannot adequately represent the sizable response of deep convection to the imposed dry layer.

4. Discussion and conclusions

The present work addresses the issue of tropical convection sensitivity to moisture variability at mid to upper levels. Its focus in this regard is the significance of dry

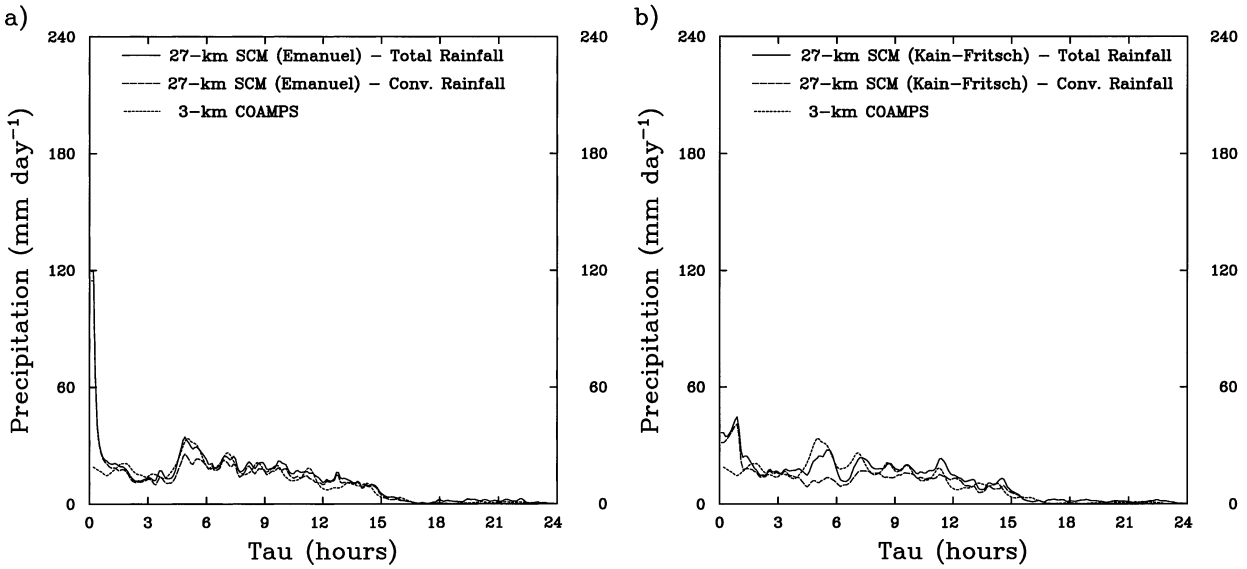

FIG. 20. Precipitation (in mm day^{-1}) obtained in 27-km-resolution SCM forecasts for Forecast B with the convective schemes of (a) Emanuel and (b) Kain–Fritsch. Corresponding results from the COAMPS 3-km mesh grid in Forecast B are also shown.

TABLE 3. Rainfall totals from the COAMPS 3-km mesh and SCM forecasts in mm.

	COAMPS 3D forecast		Emanuel SCM forecast		Kain–Fritsch SCM forecast	
Rainfall (mm)	A	B	A	B	A	B
Total	16.7	10.6	17.7	13.0	17.4	12.1
Convective			12.1	11.4	10.1	9.5
Grid scale			5.6	1.6	7.3	2.6

anomalies associated with the episodic intrusions of dry air into the Tropics from higher latitudes, the so-called dry tongues (e.g., Yoneyama and Fujitani 1995; Mapes and Zuidema 1996; Lucas and Zipser 1996). The first part of this study (section 2) investigates, through a series of numerical forecast experiments, the extent to which dry mid- to upper-level air associated with such events can inhibit deep convection, and in particular convective rainfall. The forecasts are carried out using COAMPS nested down to a 3-km mesh grid so as to at least crudely resolve deep convective circulations. Although recent modeling studies have emphasized the importance of low-level moisture for tropical convection (Lucas et al. 2000; Tompkins 2001), the present work is motivated by the observed correlation between moisture at mid to upper levels and rainfall during TOGA COARE (Brown and Zhang 1997).

In addressing the inhibitory potential of dry layers on deep convection, it must be recognized that various factors can be expected to act concurrently in this regard. Mapes and Zuidema (1996), for example, present evidence supporting the hypothesis that radiative heating profiles associated with dry tongue episodes tend to stabilize the base of the dry layer, inhibiting convection from penetrating into the dry air. Nonetheless, observations show that except for brief periods, clouds with tops at low to middle levels (and occasionally higher) do occur during the dry episodes (Brown and Zhang 1997; Parsons et al. 2000). Ultimately, one hopes to determine whether the dry air is an important factor that limits the growth of these clouds, or whether they are simply limited in growth by the characteristics of the boundary layer turbulence from which they arise (Mapes 2000). Another consideration is the potential significance of dryness near the periphery of dry tongues in inhibiting the spread of deep convection into the dry tongue interior (cf. Brown and Zhang 1997).

The experiments described in section 2 are carried out using moisture profiles from a dry tongue episode during TOGA COARE to perturb the lateral boundary conditions of the inner (3 km) mesh grid in COAMPS forecasts of convection in the tropical Pacific. The results obtained support the view that dryness at mid to upper levels associated with dry tongues can have a significant inhibitory effect on precipitation formation. Such an effect would owe particularly to the large amplitude of the relative humidity variations at those levels, as observed for TOGA COARE (Brown and Zhang 1997). Comparisons with somewhat contrasting results obtained by Lucas et al. (2000) and Tompkins (2001) are discussed in section 2. Such differences can result from differences in parcel buoyancy (cf. Kain and Fritch 1990), shear profile, and the height variability of the moisture perturbations used for testing. For example, for low-shear conditions in the mid troposphere such as in the study by Tompkins (2001), the amount of mixing between the cloud and the environment is likely to be reduced, as well as the associated sensitivity to environmental moisture variations. In regards to parcel

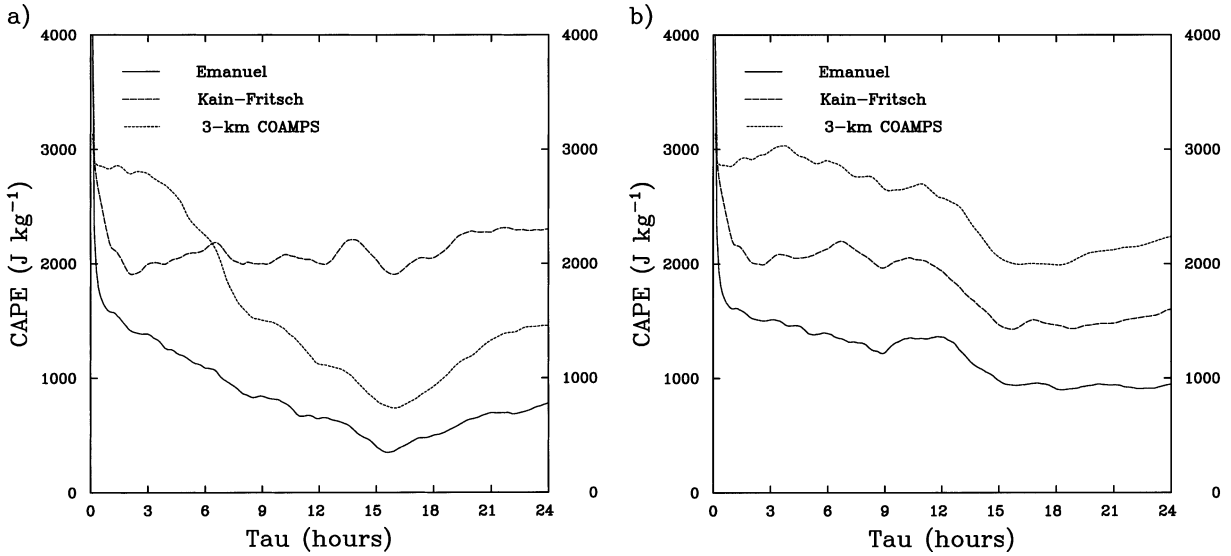

FIG. 21. CAPE (in J kg^{-1}) in the 27-km-resolution SCM forecasts corresponding to (a) Forecast A; (b) Forecast B. The corresponding values of CAPE from the COAMPS 3-km mesh grid in Forecasts A and B are also plotted.

buoyancies, there is a consideration of relevance here beyond the basic implications of the buoyancy-sorting model addressed by Kain and Fritsch (1990). One might expect that the large values of CAPE in the present simulations would produce stronger updrafts than weakly buoyant conditions, and would thus tend to reduce the production of rainfall at lower levels associated with collision-coalescence processes, and enhance the sensitivity of precipitation production to entrainment of midlevel air (cf. Zipser and LeMone 1980; DeMott and Rutledge 1998). This explanation is consistent with the results presented in Fig. 8. Similarly, the importance of cold rain processes in association with high parcel buoyancies is apparent in TOGA COARE data (DeMott and Rutledge 1998). However, there were also cases during TOGA COARE in which parcel buoyancies were low, and precipitation production was enhanced at lower levels (DeMott and Rutledge 1998). One might expect lesser sensitivity of convective rainfall in such cases to dry air entrainment at mid levels than observed here.

Although most of the inhibitory effect of mid- to upper-level dryness on precipitation observed here appears to be due directly to increased evaporation, plots of simulated updraft core mass flux (Fig. 14) suggest that a reduction in updraft mass flux near cloud-base level plays a role as well. Comparing Forecasts A and B of section 2, Forecast B (with a drier atmosphere above 600 hPa compared with Forecast A), has a 12% lower updraft mass flux than Forecast A at 900 hPa. The 900-hPa vertical moisture flux is reduced as well in Forecast B, by 10% with respect to that in Forecast A. This reduction represents 27% of the 37% reduction in surface rainfall in Forecast B.

As with all modeling studies the limitations of the numerical model and experimental design must not be overlooked. There are uncertainties, for example, concerning the extent to which inadequacies in the model physics, such as the microphysical scheme or the radiation treatment could impact the results. In addition, the use of a 3-km horizontal grid dimension for the innermost mesh in the COAMPS forecasts is not adequate to explicitly resolve much of the horizontal structure and mixing in clouds. In as much as the present study demonstrates the qualitative impact of enhanced evaporation associated with the presence of dry layers aloft, there is a reason to believe that similar results would be obtained for higher resolution simulations, perhaps with even greater sensitivities than observed here. For example, simulation results presented by Weisman et al. (1997) for midlatitude squall-line-type convection show greater evaporation of rainwater as a fraction of total condensate over 6-h forecasts for a 1-km horizontal grid dimension than for a 12-km grid dimension. As noted in section 2, the present simulations were run without any subgrid-scale horizontal turbulent mixing. Sensitivity tests showed that when this mixing is included there is a small reduction in the amount of convective precipitation, but the results are essentially unchanged. The use of a somewhat coarse grid here afforded the opportunity to carry out a number of experiments and to assimilate data for several days over a considerable area.

As for the experimental design, the imposition of the dry layer above 800 hPa during the final 24 h of the spinup process for Forecasts A and B of section 2 has the effect of permitting the buildup of greater CAPE in these forecasts than in the control forecast, Forecast CTL. Values of CAPE in excess of 2500 J kg^{-1} are plotted in Fig. 12 for the first several hours (extending out to about 12 h in the case of Forecast B) of Forecasts A and B. Values of CAPE in TOGA COARE appear to have rarely been in excess of about 2200 J kg^{-1}, with mean values for a variety of basic environment types generally in the range of about 500–1500 J kg^{-1} (Lucas and Zipser 2000). In contrast to Forecasts A and B, Forecast CTL had values of CAPE that were generally less than 1000 J kg^{-1} (not shown) and more consistent with TOGA COARE observations. Despite this difference however, profiles of precipitating hydrometeor mixing ratios are very similar for Forecast CTL (not shown) and Forecast A, supporting the view that the experimental design did not significantly change the characteristics of the precipitation process in this case.

Further evidence of the impact of dry air at mid to upper levels on CAPE can be seen by noting that Forecast B maintains higher values of CAPE than Forecast A, concurrent with the noted suppression of deep convection. Tests show that a major contribution to the greater CAPE in Forecast B comes from the moisture distribution, which exhibits values of specific humidity in the boundary layer that are on average about 0.0005 kg kg^{-1} greater than in Forecast A (cf. Parsons et al. 2000). This observation may have implications for the MJO. Kemball-Cook and Weare (2001) report an off-equatorial buildup of low-level moist static energy through surface evaporation, and concurrent drying of the midtroposphere associated with the beginning of MJO events. The effect of midtropospheric drying in moderating through entrainment the rate of such moistening of the boundary layer has been proposed (Kemball-Cook and Weare 2001). The present results suggest that the dry midtroposphere during these periods may, through suppression of convection, actually have a role in making possible the low-level moist static energy buildup. The effect of the dry midlevel air on convection may at least help counteract its tendency to lessen the rate of boundary layer moistening. Note that the dry anomaly associated with the suppressed phase of the MJO appears to be somewhat smaller than that associated with dry air intrusions from the subtropics. Kemball-Cook and Weare (2001), for example, present results showing a range of variation of the 500-hPa specific humidity of about 0.1 kg kg^{-1} during a composited average cycle of the MJO. This range is about one-third that associated with presumably smaller-scale variations that occurred during TOGA COARE (Brown and Zhang

1997). For comparison, note that the mean difference in 500-hPa specific humidity between Forecast A and Forecast B in the present study is 0.28 kg kg^{-1}. Although the occurrence of deep convection is reduced during the suppressed phase of the MJO cycle, it does indeed occur, and convection to at least midlevels is common (DeMott and Rutledge 1998). Based on the present results, it seems likely that the dry middle troposphere during this phase of the MJO would have some effect in inhibiting this convection. Further study is needed, owing in part to the somewhat lesser midlevel moisture variability associated with the MJO than that investigated in the present work.

The preceding discussion suggests that one factor of importance for realistic MJO behavior in general circulation models is an adequate representation of the inhibitory effect of a dry middle troposphere on convection. Current convective parameterizations may be limited in this regard, as illustrated by the SPM and SCM convective parameterization test results presented in section 3 of this study. Predicted increases in rainfall and cloud-base mass flux by both the Emanuel and Kain–Fritsch convective schemes in SPM forecasts when moisture at mid levels is decreased stand in contrast to decreases in these quantities in the COAMPS 3-km mesh grid forecasts used as forcing and validation data for the column tests. Similar results (not shown) were obtained in corresponding SPM tests with the relaxed Arakawa–Schubert convective parameterization (Moorthi and Suarez 1992).

The SPM forecast results suggest that the convective closure treatments employed in the Emanuel and Kain–Fritsch cumulus parameterizations may be oversimplified with respect to the extent of their dependence on parcel buoyancy. In this regard, one can note for example that Forecast B is found to have greater values of CAPE than are obtained in the moister (at mid levels) Forecast A (Fig. 12). The convective parameterizations respond to the increased parcel buoyancy in Forecast B by predicting greater cloud-base updraft mass fluxes in the SPM tests for that forecast, contrary to the COAMPS forecast results. In the case of the Emanuel scheme in particular, this failure can not be attributed to problems with the buoyancy-sorting mixing scheme because the cloud-base mass flux computation in the SPM tests is independent of the parameterized mixing.

The effectiveness of the parameterized updraft/environment mixing schemes in the Emanuel and Kain–Fritsch parameterizations was examined by comparing predictions of total updraft mass flux in the SPM forecasts (Figs. 17 and 18) with plots of this quantity computed for updraft cores from the COAMPS forecasts (Fig. 14). One finds that the Emanuel scheme tends to underpredict the amount of net detrainment at midlevels, whereas the Kain–Fritsch scheme tends to overpredict this detrainment. The lesser amount of detrainment with the Emanuel scheme may be due to the fact that it explicitly accounts for the mixing of undilute air with the environment throughout the depth of the cloud. This approach can be expected to produce a greater tendency for buoyant mixtures of cloudy and environmental air in the buoyancy-sorting computations.

Although the rainfall predictions in the SCM experiments are better than in the SPM tests, there appears to be a significant underprediction of convective rainfall in the case of Forecast A. Problems apparent from the SPM tests are also manifested in significant errors in the simulated values of CAPE (Fig. 21). Because there are no feedbacks in the SCM forecasts to the advective tendencies, there remains some uncertainty as to the extent of the model parameterization deficiencies.

The column tests described here provide a look at the horizontal scale sensitivity associated with the convective parameterization schemes. It has been noted that the buoyancy-sorting mechanism implemented in the Emanuel and Kain–Fritsch schemes is very sensitive to the local environment of the cloud. In addition, the degree of parameterizability of a convective event can be expected to decrease (or vanish altogether) as horizontal resolution is reduced. In the present study for example, there is a resolution dependence in the SPM results that supports the conclusion that the 216-km resolution tested in section 3 is too coarse for the Kain–Fritsch convective parameterization to adequately represent the deep convection in this case. Similar results (not shown) were obtained with the relaxed Arakawa–Schubert convective parameterization. These results illustrate the importance of horizontal-scale considerations for field experiment planning and data application.

Acknowledgments. The author would like to thank Duane Waliser for some helpful discussions. Comments and suggestions by the anonymous reviewers were also helpful. This research was sponsored by the Office of Naval Research, through the Naval Research Laboratory, Program Element 0601153N. The work was supported in part by a grant of computing time from the Department of Defense's High Performance Computing Program.

REFERENCES

Arakawa, A., and W. H. Schubert, 1974: Interaction of a cumulus cloud ensemble with the large-scale environment, Part I. *J. Atmos. Sci.,* **31,** 674–701.

Brown, R. G., and C. Zhang, 1997: Variability of midtropospheric moisture and its effect on cloud-top height distribution during TOGA COARE. *J. Atmos. Sci.,* **54,** 2760–2774.

Bryan, G. H., and J. M. Fritsch, 2000: The vertical distribution of humidity: A crucial factor in the organization of convection. Preprints, *20th Conf. on Severe Local Storms*, Orlando, FL, Amer. Meteor. Soc., 630–633.

Churchill, D. D., and R. A. Houze Jr., 1984: Development and structure of winter monsoon cloud clusters on 10 December 1978. *J. Atmos. Sci.,* **41,** 933–960.

Ciesielski, P. E., L. M. Hartten, and R. H. Johnson, 1997: Impacts of merging profiler and rawinsonde winds on TOGA COARE analyses. *J. Atmos. Oceanic Technol.,* **14,** 1264–1279.

Davies, H. C., 1976: A lateral boundary formulation for multi-level prediction models. *Quart. J. Roy. Meteor. Soc.,* **102,** 405–418.
DeMott, C. A., and S. A. Rutledge, 1998: The vertical structure of TOGA COARE convection. Part II: Modulating influences and implications for diabatic heating. *J. Atmos. Sci.,* **55,** 2748–2762.
Emanuel, K. A., 1991: A scheme for representing cumulus convection in large-scale models. *J. Atmos. Sci.,* **48,** 2313–2335.
——, 1994: *Atmospheric Convection.* Oxford University Press, 580 pp.
——, and M. Zivkovic-Rothman, 1999: Development and evaluation of a convection scheme for use in climate models. *J. Atmos. Sci.,* **56,** 1766–1782.
Esbensen, S., 1978: Bulk thermodynamic effects and properties of small tropical cumuli. *J. Atmos. Sci.,* **35,** 826–831.
Ferrier, B. S., 1988: One-dimensional time-dependent modeling of squall-line convection. Ph.D. thesis, University of Washington, 259 pp.
Fritsch, J. M., and C. F. Chappell, 1980: Numerical prediction of convectively driven mesoscale pressure systems. Part I: Convective parameterization. *J. Atmos. Sci.,* **37,** 1722–1733.
Fuelberg, H. E., and D. G. Biggar, 1994: The preconvective environment of summer thunderstorms over the Florida Panhandle. *Wea. Forecasting,* **9,** 316–326.
Gilmore, M. S., and L. J. Wicker, 1998: The influence of midtropospheric dryness on supercell morphology and evolution. *Mon. Wea. Rev.,* **126,** 943–958.
Harshvardhan, R. Davies, D. Randall, and T. Corsetti, 1987: A fast radiation parameterization for atmospheric circulation models. *J. Geophys. Res.,* **92,** 1009–1015.
Hodur, R. M., 1997: The Naval Research Laboratory's Coupled Ocean/Atmosphere Mesoscale Prediction System (COAMPS). *Mon. Wea. Rev.,* **125,** 1414–1430.
Hogan, T. F., and T. E. Rosmond, 1991: The description of the U.S. Navy Operational Global Atmospheric Prediction System's spectral forecast model. *Mon. Wea. Rev.,* **119,** 1786–1815.
Johnson, R. H., 1978: Cumulus transports in a tropical wave composite for phase-III of GATE. *J. Atmos. Sci.,* **35,** 484–494.
Jones, C., D. E. Waliser, J. K. E. Schemm, and W. K. M. Lau, 2000: Prediction skill of the Madden and Julian Oscillation in dynamical extended range forecasts. *Climate Dyn.,* **16,** 273–289.
Kain, J. S., and J. M. Fritsch, 1990: A one-dimensional entraining/detraining plume model and its application in convective parameterization. *J. Atmos. Sci.,* **47,** 2784–2802.
Kalnay, E., and R. Jenne, 1991: Summary of the NMC/NCAR reanalysis. *Bull. Amer. Meteor. Soc.,* **72,** 1897–1904.
——, and Coauthors, 1993: The NMC/NCAR CDAS/Reanalysis Project. NMC Office Note 401, 289 pp.
Kemball-Cook, S. R., and B. C. Weare, 2001: The onset of convection in the Madden–Julian Oscillation. *J. Climate,* **14,** 780–793.
Kuo, H. L., 1974: Further studies of the parameterization of the influence of cumulus convection on large-scale flow. *J. Atmos. Sci.,* **31,** 1232–1240.
LeMone, M. A., and E. J. Ziper, 1980: Cumulonimbus vertical velocity events in GATE. Part I: Diameter, intensity and mass flux. *J. Atmos. Sci.,* **37,** 2444–2457.
Louis, J. F., M. Tiedtke, and J. F. Geleyn, 1982: A short history of the operational PBL-parameterization at ECMWF. *Proc. Workshop on Planetary Boundary Parameterization,* Reading, United Kingdom, ECMWF, 59–79.
Lucas, C., and E. J. Zipser, 1996: The impact of dry air intrusions on mesoscale convective systems. Preprints, *Eighth Conf. on Air–Sea Interaction,* Atlanta, GA, Amer. Meteor. Soc., J132–J133.
——, and ——, 2000: Environmental variability during TOGA COARE. *J. Atmos. Sci.,* **57,** 2333–2350.
——, ——, and B. S. Ferrier, 2000: Sensitivity of tropical West Pacific oceanic squall lines to tropospheric wind and moisture profiles. *J. Atmos. Sci.,* **57,** 2351–2373.
Maloney, E. D., and D. L. Hartmann, 2001: The sensitivity of intraseasonal variability in the NCAR CCM3 to changes in convective parameterization. *J. Climate,* **14,** 2015–2034.
Mapes, B. E., 2000: Convective inhibition, subgrid-scale triggering energy, and stratiform instability in a toy tropical wave model. *J. Atmos. Sci.,* **57,** 1515–1535.
——, and P. Zuidema, 1996: Radiative-dynamical consequences of dry tongues in the tropical troposphere. *J. Atmos. Sci.,* **53,** 620–638.
Mellor, G., and T. Yamada, 1974: A hierarchy of turbulence closure models for planetary boundary layers. *J. Atmos. Sci.,* **31,** 1791–1806.
Moorthi, S., and M. J. Suarez, 1992: Relaxed Arakawa–Schubert: A parameterization of moist convection for general circulation models. *Mon. Wea. Rev.,* **120,** 978–1002.
Numaguti, A., R. Oki, K. Nakamura, K. Tsuboki, N. Misawa, T. Asai, and Y.-M. Kodama, 1995: 4–5-day-period variations and low-level dry air observed in the equatorial western Pacific during the TOGA-COARE IOP. *J. Meteor. Soc. Japan,* **73,** 267–290.
Parsons, D. B., K. Yoneyama, and J. L. Redelsperger, 2000: The evolution of the tropical western Pacific atmosphere–ocean system following the arrival of a dry intrusion. *Quart. J. Roy. Meteor. Soc.,* **126,** 517–548.
Petch, J. C., and J. Dudhia, 1998: The importance of horizontal advection of hydrometeors in a single column model. *J. Climate,* **11,** 2437–2452.
Randall, D. A., K.-M. Xu, R. J. C. Somerville, and S. Iacobellis, 1996: Single-column models and cloud ensemble models as links between observations and climate models. *J. Climate,* **9,** 1683–1697.
Raymond, D. J., and A. M. Blyth, 1986: A stochastic mixing model for nonprecipitating cumulus clouds. *J. Atmos. Sci.,* **43,** 2708–2718.
Rutledge, S. A., and P. V. Hobbs, 1983: The mesoscale and microscale structure of organization of clouds and precipitation in midlatitude cyclones. Part VIII: A model for the ''seeder-feeder'' process in warm-frontal rainbands. *J. Atmos. Sci.,* **40,** 1185–1206.
Sheu, R.-S., and G. Liu, 1995: Atmospheric humidity variations associated with westerly wind bursts during Tropical Ocean Global Atmosphere (TOGA) Coupled Ocean Atmosphere Response Experiment (COARE). *J. Geophys. Res.,* **100,** 25 759–25 768.
Simpson, J., 1983: Cumulus clouds: Early aircraft observations and entrainment hypotheses. *Mesoscale Meteorology—Theories, Observations and Models,* D. K. Lilly and T. Gal-Chen, Eds., D. Reidel, 355–373.
Slingo, J. M., 1987: The development and verification of a cloud prediction scheme for the ECMWF model. *Quart. J. Roy. Meteor. Soc.,* **113,** 899–927.
——, and Coauthors, 1996: Intraseasonal oscillations in 15 atmospheric general circulation models: Results from an AMIP diagnostic subproject. *Climate Dyn.,* **12,** 325–357.
Stommel, H., 1947: Entrainment of air into a cumulus cloud. *J. Meteor.,* **4,** 91–94.
Tompkins, A. M., 2001: Organization of tropical convection in low vertical wind shears: The role of water vapor. *J. Atmos. Sci.,* **58,** 529–545.
Webster, P. J., and R. Lukas, 1992: TOGA COARE: The coupled ocean–atmosphere response experiment. *Bull. Amer. Meteor. Soc.,* **73,** 1377–1416.
Weisman, M. L., W. C. Skamarock, and J. B. Klemp, 1997: The resolution dependence of explicitly modeled convective systems. *Mon. Wea. Rev.,* **125,** 527–548.
Yoneyama, K., and T. Fujitani, 1995: The behavior of dry westerly air associated with convection observed during the TOGA-COARE R/V Natsushima cruise. *J. Meteor. Soc. Japan,* **73,** 291–304.
Zipser, E. J., and M. A. LeMone, 1980: Cumulonimbus vertical velocity events in GATE. Part II: Synthesis and model core structure. *J. Atmos. Sci.,* **37,** 2458–2469.